
LAGO: Language-Guided Adaptive Object-Region Focus for Zero-Shot Visual–Text Alignment

Junyi Hu^{1,2,3*} Qiji Zhou^{2*} Lei Zhang¹ Yue Zhang^{2†}

¹Beijing Jiaotong University ²Westlake University ³Rochester Institute of Technology
jh7132@rit.edu yue.zhang@wias.org.cn

Abstract

Zero-shot recognition aims to classify an image by selecting the most compatible label description from a set of candidate classes without any task-specific supervision. In fine-grained settings, however, the relevant evidence often lies in localized parts, attributes, or textures rather than in the full image, making whole-image alignment suboptimal. Recent localized visual-text alignment methods address this by comparing class descriptions with multiple image regions, but they typically rely on large sets of random or redundant crops, increasing inference cost and introducing many highly redundant or weakly relevant candidates. Moreover, introducing semantic guidance too early can create an error-amplifying feedback process in which inaccurate intermediate predictions bias later localization and reinforce subsequent mistakes; we refer to this failure mode as the *prediction loop*. We propose **LAGO** (**L**anguage-**G**uided adaptive **O**bject-region **f**ocus), a framework for efficient and robust zero-shot localized visual-text alignment. LAGO first performs class-agnostic object-centric candidate discovery to obtain a stable visual initialization, and then applies adaptive language-guided refinement with the strength of semantic guidance controlled by intermediate confidence. It further combines object-level, contextual, and full-image evidence through an effective object-context dual-channel aggregation strategy. Extensive experiments show that LAGO consistently achieves state-of-the-art performance on standard zero-shot benchmarks and challenging distribution-shift settings, while requiring substantially fewer candidate regions at inference time. Code is available [here](#).

1 Introduction

Zero-shot recognition can be naturally viewed as a visual-text alignment problem over a candidate label set. Given an image and a set of class names or descriptions, the model selects the label from the candidate set whose textual semantics best align with the visual content. Following the success of CLIP, zero-shot recognition has largely been implemented by directly matching text embeddings against a single fixed global image representation [1–3]. While effective, global alignment is often insufficient for fine-grained recognition, where decisive evidence may lie in localized object parts, attributes, or textures rather than in the image as a whole [4–6]. In these cases, the key problem is not only how to enrich class descriptions, but also how to align them with the right visual regions [4, 5, 7].

This problem has motivated recent efforts toward localized visual-text alignment. In particular, methods such as WCA [6], BiFTA [8], and FG-CLIP [9] show that fine-grained class descriptions are often better matched with regional visual evidence than with a single global representation. However, these methods still largely rely on large sets of random or overcomplete crops followed by crop-level similarity aggregation [6, 8, 10]. This improves coverage, but also introduces redundancy and weakly

*Equal contribution.

†Corresponding author.

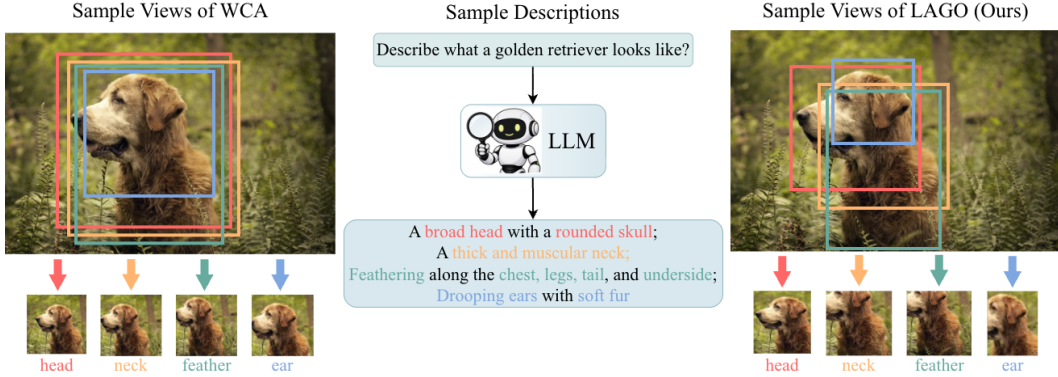


Figure 1: **Visual-text alignment for zero-shot label selection.** Given an image and a candidate class (e.g., *golden retriever*), the model first derives fine-grained class descriptions (center), then searches for visual regions that closely correspond to these semantic cues, and finally decides whether the image matches the label. Compared with WCA (left) [6], which relies on random crop sampling, LAGO (right) discovers a compact set of object-centric regions that more faithfully correspond to the described attributes, enabling substantially more accurate and efficient zero-shot recognition.

relevant views. Thus, the main bottleneck is not text enrichment alone, but effective region discovery: how to identify a compact set of visually informative and semantically relevant regions for alignment.

To address this bottleneck, we propose **LAGO** (**L**anguage-**G**uided adaptive **O**bject-region focus), a framework for efficient and robust zero-shot localized visual-text alignment. As illustrated in Figure 1, LAGO replaces random crop enumeration with a compact set of object-centric regions that better correspond to fine-grained semantic cues. Compared with prior crop-based localized alignment [6], LAGO aims to explicitly focus the model on stable object regions first, and then use language to adaptively refine region selection only when the intermediate prediction becomes sufficiently reliable.

Language-guided region discovery is nontrivial in zero-shot recognition. At the beginning of inference, target semantics are uncertain because the model does not yet know the correct class. Early predictions may therefore be unreliable. If used too aggressively to guide localization, they may steer the model toward misleading regions and reinforce the same error during later refinement. We refer to this error-amplifying feedback between recognition and localization as the *prediction loop*. LAGO avoids this failure mode with a confidence-aware two-stage strategy. It first performs class-agnostic object-centric candidate discovery to obtain a stable visual initialization, and then applies adaptive text-guided refinement whose strength is controlled by intermediate confidence. High-confidence samples receive stronger semantic focusing, whereas low-confidence samples retain more diverse candidates to avoid premature commitment. LAGO further jointly combines object-focused regions, contextual evidence, and full-image representations through an object-context dual-channel aggregation strategy.

Extensive experiments on standard zero-shot benchmarks and challenging natural distribution-shift settings show that LAGO consistently outperforms representative recent methods while using substantially fewer candidate regions at inference time. The gains are especially pronounced on fine-grained and texture-sensitive datasets, where localized evidence matters most, and remain consistent under natural distribution shifts, indicating that confidence-aware refinement improves both recognition accuracy and robustness in practice. Our main contributions are twofold: (i) we identify semantic over-conditioning during zero-shot region discovery as an error-amplifying failure mode, termed the *prediction loop*; and (ii) we propose LAGO, a confidence-aware localized alignment framework that systematically combines class-agnostic initialization, sample-adaptive text-guided refinement, and object-context aggregation, achieving stronger zero-shot recognition with fewer candidate regions.

2 Related Work

Textual supervision and global zero-shot alignment. A broad line of research improves zero-shot recognition by enriching the textual supervision used in vision-language models beyond plain class names. This includes prompt learning and prompt regularization methods that adapt text representa-

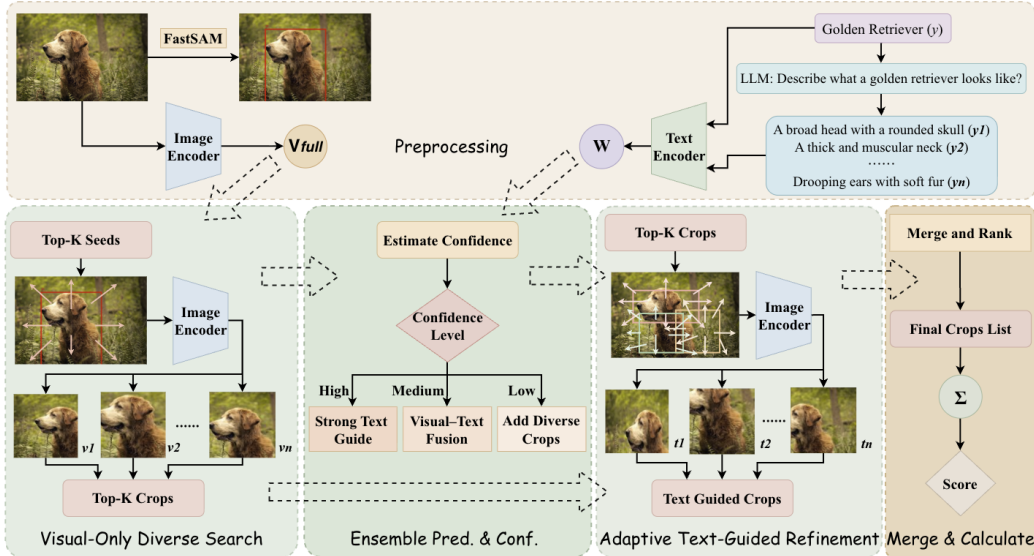


Figure 2: **Overview of LAGO.** The pipeline consists of preprocessing (§3.1), visual-only diverse search (§3.2), ensemble prediction & confidence and adaptive text-guided refinement (§3.3); and merge & calculate (§3.4). Further implementation details of our method are provided in Appendix A.

tions with learnable contexts, as well as training-free approaches that exploit LLM-generated class descriptions containing fine-grained semantic cues such as object parts, attributes, and contextual properties [2–5, 7, 11–18]. Despite their differences in how textual supervision is constructed, these methods largely align enriched class semantics with a single global image representation. Consequently, they remain limited when the evidence needed for recognition is inherently localized. LAGO addresses this by applying text supervision to object-focused regions instead of the whole image.

Localized visual-text alignment. Closest to our setting, recent work shows that fine-grained descriptions often align better with regional visual evidence than whole-image features in zero-shot recognition [6, 8, 9, 19, 20]. WCA aggregates similarities between class descriptions and image crops, while BiFTA reduces redundancy in sampled visual and textual representations through bi-refinement before cross-alignment [6, 8]. These methods validate localized alignment, but still begin with large sets of random or overcomplete crops and recover evidence through refinement or aggregation. Our method targets region discovery itself. We replace exhaustive crop enumeration with a confidence-aware two-stage framework that separates class-agnostic object-centric initialization from adaptive semantic refinement, producing stable localized alignment, reducing reliance on large candidate pools, and mitigating the *prediction loop*. More broadly, our design starts from class-agnostic object-centric candidates, introduces semantic guidance adaptively, and retains contextual and full-image evidence.

Inference-time refinement and language-guided localization. Related ideas also appear in inference-time refinement and language-guided localization. Inference-time methods for CLIP-like models refine prompts, predictions, calibration, or view aggregation during test time to improve robustness under distribution shift [21–26]. Meanwhile, visual search, grounding, and referring-expression methods demonstrate that language can effectively guide localization when a reliable query is available [27–39]. Our setting differs from both lines of work: we do not refine prompts or logits, and unlike grounding, we do not simply begin with a trustworthy target query. Instead, we study zero-shot localized alignment under *latent target semantics*, where semantic guidance must be introduced carefully to avoid the *prediction loop*. This motivates our confidence-aware two-stage design, which delays semantic conditioning until a stable visual initialization has been established.

3 Method

As shown in Figure 2, the pipeline consists of four stages. In the *Preprocessing* stage (§3.1), LAGO extracts full-image features, generates object proposals with FastSAM [40], and encodes LLM-generated class descriptions as text features. The *Visual-Only Diverse Search* stage (§3.2)

implements class-agnostic object-centric initialization, constructing a compact and diverse set of proposal-centered visual regions. The *Ensemble Prediction & Confidence Estimation* and *Adaptive Text-guided Refinement* blocks implement confidence-aware two-stage region discovery (§3.3), where visual-only localization provides a prediction and confidence controls the strength of text-guided refinement. Finally, the *Merge & Calculate* stage (§3.4) performs object-context dual-channel aggregation by combining object-focused regions, contextual crops, and the full-image prediction.

3.1 Preliminaries

Let x denote an input image and let \mathcal{Y} denote the candidate class set. We use a frozen pre-trained CLIP model with an image encoder E_I and a text encoder E_T [1]. For each class $y \in \mathcal{Y}$, LAGO encodes its textual description q_y as $\mathbf{t}_y = E_T(q_y) \in \mathbb{R}^d$. For each image crop c , it encodes the visual content as $\mathbf{v}(c) = E_I(c) \in \mathbb{R}^d$. Crop-level image-text alignment is measured by cosine similarity,

$$s(c, y) = \text{sim}(\mathbf{v}(c), \mathbf{t}_y). \quad (1)$$

3.2 Class-Agnostic Object-Centric Candidate Initialization

A central challenge in zero-shot localized alignment is that reliable class semantics are often unavailable at the beginning of inference. Directly using early class predictions to guide localization may therefore, in practice, bias region selection toward misleading visual evidence during subsequent refinement. To avoid this failure mode, LAGO begins with *class-agnostic* candidate initialization.

For each image, we first obtain a small set of object-centric candidate proposal boxes,

$$\mathcal{B}_0 = \{b_1^{(0)}, b_2^{(0)}, \dots, b_M^{(0)}\}, \quad (2)$$

using an off-the-shelf proposal generator [41]. Each proposal serves as a starting point for proposal-centered local visual exploration in bounding-box space. The goal of this stage is not to determine the precise final semantic target, but to construct a compact yet diverse set of visually salient, object-centric candidate regions that provides a stable and reliable initialization for later refinement.

Let $\mathcal{C}^{(0)}$ denote the final resulting candidate set after proposal-centered search and redundancy suppression. Compared with exhaustive random cropping, this design substantially narrows the search space to a smaller, more informative, and more stable set of candidate views. In the main paper, we treat proposal-centered search as a simple candidate initialization mechanism; the complete search procedure and practical implementation details are also provided in the Appendix A.2.

3.3 Confidence-Aware Two-Stage Region Discovery

Even with a compact candidate set, semantic guidance cannot be introduced naively in zero-shot recognition. If early intermediate predictions are used too aggressively to steer localization, the model may repeatedly focus on misleading visual evidence and thereby further amplify the same error during later refinement. We refer to this error-amplifying failure mode as the *prediction loop*. LAGO explicitly addresses this issue through a confidence-aware two-stage region discovery strategy.

Scoring functions. For each candidate box b , LAGO assigns a visual score and a text score:

$$S_{\text{visual}}(b) = p(b) \quad (3)$$

$$S_{\text{text}}(b) = q(b) = \text{sim}(\mathbf{v}(b), \mathbf{w}_{\text{text}}). \quad (4)$$

Here, $S_{\text{visual}}(b)$ captures the class-agnostic crop quality, and $S_{\text{text}}(b)$ captures the class-conditional semantic relevance to the text prototype. Both are later reused in downstream crop aggregation.

Stage 1: visual-only localization. The first stage is entirely class-agnostic. Given a candidate box b , we score it using only visual evidence, without relying on any class-level semantic predictions,

$$S^{(1)}(b) = S_{\text{visual}}(b), \quad (5)$$

which corresponds to setting the semantic guidance weight to zero throughout this stage. This stage identifies visually salient and object-centric regions without relying on uncertain class predictions at this early stage. Let the resulting candidate set for subsequent refinement be denoted by $\mathcal{C}^{(1)}$.

Algorithm 1: Confidence-Aware Two-Stage Region Discovery

Require: image x , proposal set \mathcal{B}_0 , full-image feature \mathbf{v}_{full} , class text bank \mathbf{W}

Ensure: final crop set \mathcal{C} , confidence c , prediction \hat{y}

```
1 Function TWOSTAGEREGIONDISCOVERY( $x, \mathcal{B}_0, \mathbf{v}_{\text{full}}, \mathbf{W}$ )
   // Stage 1: class-agnostic candidate discovery
2    $\mathcal{C}^{(1)} \leftarrow \bigcup_{b \in \mathcal{B}_0} \text{SEARCHTOPKCROPS}(x, b, \mathbf{v}_{\text{full}}, \text{None}, 0)$ 
   // Intermediate prediction and confidence
3    $\mathbf{v}_{\text{ens}} \leftarrow \text{MEANPOOLTOPCROPS}(\mathcal{C}^{(1)})$ 
4    $\mathbf{z}^{(1)} \leftarrow \mathbf{v}_{\text{ens}}^\top \mathbf{W}$ 
5    $(\hat{y}, c) \leftarrow \text{PREDICTIONCONFIDENCE}(\mathbf{z}^{(1)})$ 
6    $\gamma \leftarrow \psi(c)$ 
7    $\mathbf{w}_{\text{text}} \leftarrow \text{CONSTRUCTTEXTPROTOTYPE}(\mathbf{z}^{(1)}, \mathbf{W})$ 
   // Stage 2: adaptive text-guided refinement
8    $\mathcal{C}^{(2)} \leftarrow \bigcup_{b \in \text{TOPBOXES}(\mathcal{C}^{(1)})} \text{SEARCHTOPKCROPS}(x, b, \mathbf{v}_{\text{full}}, \mathbf{w}_{\text{text}}, \gamma)$ 
   // Merge and rank final crops
9    $\mathcal{C} \leftarrow \text{MERGEANDREFINE}(\mathcal{C}^{(1)}, \mathcal{C}^{(2)}, x, \mathbf{w}_{\text{text}}, \gamma)$ 
10   $\mathcal{C} \leftarrow \text{RANKCROPS}(\mathcal{C})$ 
11  return  $\mathcal{C}, c, \hat{y}$ 
```

Using the top-ranked regions in $\mathcal{C}^{(1)}$, we compute an initial crop-based prediction and obtain intermediate logits $\mathbf{z}^{(1)} \in \mathbb{R}^{|\mathcal{Y}|}$. We then estimate an intermediate confidence score from these logits

$$c = \phi(\mathbf{z}^{(1)}), \quad (6)$$

where $\phi(\cdot)$ can be instantiated as a simple softmax-based or margin-based confidence measure.

Stage 2: adaptive semantic refinement. In the second stage, we refine region discovery by incorporating text relevance into the scoring objective. Crucially, the strength of semantic guidance is not fixed, but is instead adaptively controlled by the sample-specific intermediate confidence score:

$$\gamma = \psi(c), \quad (7)$$

where $\psi(\cdot)$ is a monotone mapping from confidence to semantic-guidance strength for each individual test sample at inference time. The refined scoring function is then formally given below by

$$S^{(2)}(b) = (1 - \gamma) S_{\text{visual}}(b) + \gamma S_{\text{text}}(b). \quad (8)$$

This design introduces semantic refinement only after a stable visual initialization has been established. High-confidence samples receive stronger text-guided focusing, whereas low-confidence samples preserve greater reliance on visual evidence and candidate diversity. In this way, LAGO benefits from semantic guidance without allowing unreliable early predictions to prematurely dominate localization.

Algorithm 1 summarizes the overall inference flow of the confidence-aware two-stage procedure. The low-level proposal-centered search subroutine is treated as an implementation detail and deferred to Appendix A.2, where the complete candidate region discovery process is described in Algorithm 2.

3.4 Object-Context Dual-Channel Aggregation

Localized alignment improves fine-grained recognition, but object crops alone may miss context [38]. LAGO therefore aggregates object, context, and full-image evidence through a dual-channel design.

After region discovery, valid crops are divided into an object channel \mathcal{C}_o and a context channel \mathcal{C}_c , while the full image contributes separately via \mathbf{z}_{full} . For each crop c_i , let $\mathbf{s}_i \in \mathbb{R}^{|\mathcal{Y}|}$ denote its crop-level class similarity vector. Using the introduced visual and text scores from Sec. 3.3,

$$S_{\text{visual}}(c_i) = p(c_i), \quad S_{\text{text}}(c_i) = q(c_i) = \text{sim}(\mathbf{v}(c_i), \mathbf{w}_{\text{text}}), \quad (9)$$

we normalize them within each channel $\kappa \in \{o, c\}$ to make the resulting weights directly comparable:

$$p_i^{(\kappa)} = \frac{\exp(S_{\text{visual}}(c_i)/\tau_v)}{\sum_{j \in \mathcal{C}_\kappa} \exp(S_{\text{visual}}(c_j)/\tau_v)}, \quad q_i^{(\kappa)} = \frac{\exp(S_{\text{text}}(c_i)/\tau_t)}{\sum_{j \in \mathcal{C}_\kappa} \exp(S_{\text{text}}(c_j)/\tau_t)}. \quad (10)$$

The crop weight is obtained by combining normalized visual and text scores within each channel.

$$w_i^{(\kappa)} = (1 - \beta) p_i^{(\kappa)} + \beta q_i^{(\kappa)}. \quad (11)$$

The two channels are first aggregated separately and subsequently fused together as follows:

$$\mathbf{z}_\kappa = \sum_{i \in \mathcal{C}_\kappa} w_i^{(\kappa)} \mathbf{s}_i, \quad \mathbf{z}_{\text{dc}} = \alpha_{\text{dc}} \mathbf{z}_o + (1 - \alpha_{\text{dc}}) \mathbf{z}_c, \quad (12)$$

followed by interpolating the dual-channel prediction with the full-image logits to obtain final logits.

$$\mathbf{z}_{\text{final}} = \lambda \mathbf{z}_{\text{dc}} + (1 - \lambda) \mathbf{z}_{\text{full}}. \quad (13)$$

4 Experiments

We evaluate LAGO on standard zero-shot recognition benchmarks, natural distribution-shift benchmarks, and a series of carefully designed ablation studies. We also provide both qualitative and comprehensive quantitative analyses of the proposed region discovery strategy in greater detail.

4.1 Experimental Setup

Datasets. We evaluate LAGO on six widely used standard zero-shot benchmarks: ImageNet [42], CUB [43], Oxford Pets [44], DTD [45], Food101 [46], and Places365 [47]. These datasets cover generic object recognition, fine-grained recognition, texture classification, food classification, and scene recognition. We also evaluate robustness on four natural distribution-shift benchmarks derived from ImageNet: ImageNet-V2 [48], ImageNet-R [49], ImageNet-S [50], and ImageNet-A [51].

Baselines. For standard zero-shot recognition, we compare with strong baselines including CLIP [1], CLIP-E [1], CuPL [5], BiFTA [8], and WCA [6]. These baselines cover representative hand-crafted prompting, LLM-based text enrichment, and localized visual-text alignment. For natural-shift evaluation, we further compare with recent prompt-learning and test-time prompting methods, including CoOp [2], CoCoOp [3], UPT [11], ProGrad [13], KgCoOp [14], TPT [21], and DiffTPT [22].

Implementation details. We instantiate LAGO on CLIP [1] with ViT-B/32, ViT-B/16, and ViT-L/14 backbones. Unless specified, experiments use a zero-shot protocol with frozen encoders and no parameter tuning. LAGO performs proposal-centered candidate initialization, confidence-aware two-stage region discovery, and object-context dual-channel aggregation. Crops are filtered with IoU-based diversity constraints, and inference uses a fixed number of views for batched evaluation. We optionally calibrate the fusion weights (β , α_{dc} , λ) per dataset using a parameter-free score-level procedure, which is not strictly training-free and is discussed separately in Appendix A.5. Experiments use a single NVIDIA A100 GPU. Full implementation details are provided in Appendix A.

Text description construction. Following prior description-based zero-shot works [4, 5, 8], we use carefully designed offline class descriptions as text supervision signals throughout inference. Their construction and optional prototype reweighting are described in full detail in Appendix A.1.

4.2 Main Results

Table 1 presents the main zero-shot classification results. Across all datasets and backbones, LAGO achieves the best performance among zero-shot methods. The improvements are pronounced on datasets where discriminative evidence is localized or fine-grained. For example, on CUB, LAGO improves over WCA by **+2.25**, **+3.19**, and **+0.99** pts across the three backbones, indicating that more reliable region discovery helps capture subtle part-level cues. On DTD, which depends heavily on texture-level evidence, the gains reach **+4.10**, **+2.42**, and **+2.12** pts, suggesting that confidence-aware refinement is beneficial when recognition relies on local visual patterns rather than global structure.

On Places365, a scene-centric benchmark where recognition relies on scene layout, contextual objects, and background cues, LAGO improves over WCA by **+1.93**, **+4.13**, and **+5.05** pts across backbones. This suggests that object-context dual-channel aggregation remains useful when context is central to recognition. On ImageNet, Oxford Pets, and Food101, gains over WCA are smaller but stable, indicating that the proposed region discovery strategy also generalizes beyond fine-grained settings.

Table 1: Comparison of zero-shot accuracy (%) across datasets using CLIP backbones.

Method	ImageNet			CUB			Oxford Pets			DTD			Food101			Place365		
	B/32	B/16	L/14	B/32	B/16	L/14	B/32	B/16	L/14	B/32	B/16	L/14	B/32	B/16	L/14	B/32	B/16	L/14
CLIP [1]	62.05	66.74	73.48	51.21	56.01	62.12	85.04	88.14	93.24	42.93	42.98	52.61	82.60	88.40	92.55	38.51	39.27	39.63
LLIP-E [1]	63.37	68.37	75.52	52.74	56.16	62.53	87.38	89.10	93.62	43.83	45.27	55.43	83.93	88.83	93.07	39.28	40.30	40.55
CLIP-D [4]	63.01	68.04	75.03	52.69	57.08	63.26	84.46	87.52	93.30	44.20	46.17	55.05	84.12	88.85	93.03	39.90	40.34	40.55
Waffle [7]	63.30	68.12	75.31	52.04	56.89	62.27	85.50	86.51	91.55	42.98	44.68	54.31	83.98	89.06	93.33	39.47	40.76	40.89
CuPL [5]	64.37	69.61	76.62	49.76	56.42	62.15	87.03	91.14	94.33	47.50	50.53	60.59	84.20	88.98	93.37	39.08	39.83	40.77
BiFTA [8]	66.83	71.14	77.82	58.24	60.06	65.67	89.74	91.67	94.96	53.22	54.64	62.45	86.43	90.11	93.97	41.55	42.12	42.98
WCA [6]	66.84	71.08	77.32	56.91	59.78	65.24	89.89	92.23	94.66	49.39	52.79	61.78	86.40	90.01	93.96	40.66	41.43	42.23
Ours	67.98	71.72	77.97	59.16	62.97	66.23	90.71	92.78	95.07	53.49	55.21	63.90	86.96	90.54	94.35	42.59	45.56	47.28
Δ	+1.14	+0.64	+0.65	+2.25	+3.19	+0.99	+0.82	+0.55	+0.41	+4.10	+2.42	+2.12	+0.56	+0.53	+0.39	+1.93	+4.13	+5.05

Table 2: Comparison on natural distribution shifts with accuracy (%) reported. TP, VP, TTP, and LLM represent textual prompting, visual prompting, test-time prompting, and large language models, respectively. The term ‘‘Tuned’’ refers to whether the model is fine-tuned on ImageNet. ‘‘Source’’ refers to in-distribution performance, while ‘‘Target’’ represents out-of-distribution performance.

Method	Prompts	Tuned?	Source	Target				Average
			ImageNet	ImageNet-V2	ImageNet-R	ImageNet-S	ImageNet-A	
CoOp [2]	TP	✓	71.51	64.20	75.21	47.99	49.71	61.72
CoCoOp [3]	VP+TP	✓	71.02	64.07	76.18	48.75	50.63	62.13
UPT [11]	VP+TP	✓	72.63	64.35	76.24	48.66	50.66	62.51
ProGrad [13]	TP	✓	<u>72.24</u>	64.73	74.58	47.99	49.39	61.79
KgCoOp [14]	TP	✓	71.20	64.10	76.70	48.97	50.69	62.33
TPT [21]	TTP	✓	69.70	64.30	73.90	46.40	53.67	61.59
DiffTPT [22]	TTP	✓	70.30	<u>65.10</u>	75.00	46.80	55.68	62.58
CLIP [1]	Hand-crafted	✗	66.74	60.83	73.96	46.15	47.77	59.09
CLIP-E [1]	Hand-crafted	✗	68.37	61.90	77.40	47.87	49.00	60.91
CuPL [5]	LLM-TP	✗	69.61	63.27	77.10	48.80	50.77	61.91
WCA [6]	LLM-TP+VP	✗	71.08	64.71	<u>78.06</u>	<u>50.18</u>	<u>56.13</u>	<u>64.03</u>
Ours	LLM-TP+VP	✗	71.72	65.90	78.91	50.81	59.16	65.30

Compared with prior localized alignment methods such as WCA and BiFTA, these results show that replacing exhaustive crop enumeration with confidence-aware semantic refinement leads to both more accurate and more stable region selection during inference under challenging zero-shot conditions.

LAGO also performs strongly under natural distribution shifts (Table 2). Compared with WCA, our method improves by **+1.19** pts on ImageNet-V2, **+0.85** pts on ImageNet-R, **+0.63** pts on ImageNet-S, and **+3.03** pts on ImageNet-A, increasing the overall average by **+1.27** pts. The gain on ImageNet-A is particularly notable, suggesting that confidence-aware region refinement is most beneficial when global representations become unreliable and discriminative cues are sparse or partially misleading.

Importantly, unlike recent prompt-learning and test-time prompting methods such as CoOp, CoCoOp, and DiffTPT shown in Table 2, LAGO consistently achieves these gains without any parameter tuning in practice. This indicates that stable candidate initialization and sample-adaptive semantic guidance still noticeably improve robustness under distribution shift even in a fully training-free setting.

In addition to these accuracy gains, LAGO requires substantially fewer candidate regions than WCA due to proposal-centered initialization and confidence-aware refinement, leading to more efficient inference across standard datasets and backbones in practice without exhaustive crop enumeration.

4.3 Analysis: Where Do the Gains Come From?

We next analyze how LAGO’s design choices affect inference beyond aggregate accuracy. We consider four aspects: candidate-region efficiency under limited region budgets, Stage-wise refinement, confidence-aware behavior, and remaining failure modes under distribution shift. Additional qualitative and human-evaluation analyses are provided for completeness in Appendix E and Appendix F.

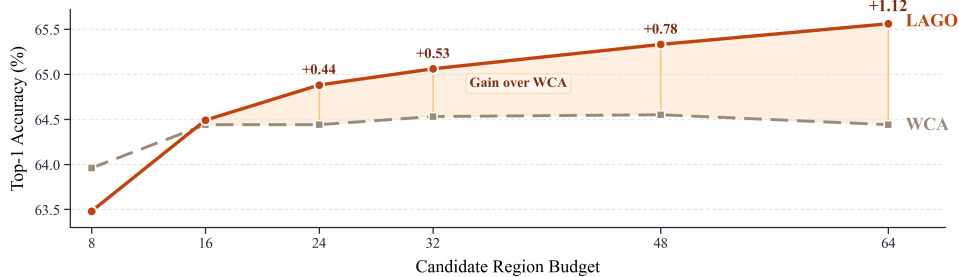


Figure 3: **Candidate-region budget analysis of LAGO.** Efficiency analysis on ImageNet-V2, showing that LAGO uses candidate regions more effectively than WCA as the budget increases.

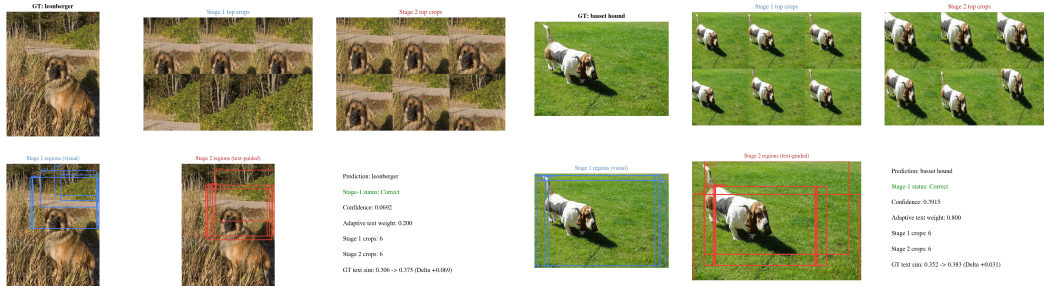


Figure 4: **Stage-wise visualization.** Each example shows the image, Stage 1/Stage 2 top crops, candidate regions, and confidence/text-similarity changes. Stage 1 selects object-centric regions, whereas Stage 2 refines them toward class-relevant evidence aligned with ground-truth text prototype.

Candidate-region efficiency. We first examine how LAGO uses a fixed inference region budget, measured as candidate regions evaluated per image at inference time. As shown in Figure 3, LAGO is slightly weaker than WCA at the smallest budget of 8 because too few regions limit proposal coverage and semantic refinement under such tight constraints. Once the budget becomes large enough for stable coverage and refinement, LAGO becomes stronger than WCA, and the gap increases as more regions are allowed. This directly suggests that LAGO benefits from informative and selective region discovery rather than exhaustive crop enumeration alone. Additional details on the candidate-region budget setting and efficiency analysis are provided in Appendix C.1 there for completeness.

Confidence-aware behavior. To understand where adaptive guidance is most beneficial, we group samples by intermediate confidence and examine adaptive-corrected cases. Among them, 77/84 (91.7%) fall in the low-confidence regime, while 7/84 (8.3%) fall in the medium-confidence regime. This indicates that most corrections occur when the initial prediction is uncertain. Compared with fixed or random crop baselines, LAGO uses confidence to adaptively control text-guided refinement, avoiding premature commitment to unreliable early predictions. This particularly highlights LAGO’s advantage under difficult cases. Representative corrected examples are provided in Appendix C.2.

Stage-wise visualization. Figure 4 illustrates how region discovery evolves from Stage 1 to Stage 2. Stage 1 identifies salient object-centric regions without relying on class semantics, while Stage 2 further shifts attention toward class-relevant and discriminative regions guided by the intermediate prediction. Compared with fixed or random crop baselines, LAGO adaptively refines regions to capture more informative visual evidence. These examples highlight the advantage of the two-stage design: it first provides a stable visual initialization and then improves localization with confidence-aware semantic guidance. Similar behavior across multiple datasets is provided in Appendix C.3.

Failure cases. We analyze failure modes on ImageNet-R, since its stylized renditions make appearance cues less consistent with semantics under distribution shift. The dominant failure mode is semantic mismatch (50.0%), followed by cluttered or poorly localized regions (21.4%), ambiguous classes (7.1%), and other cases. These observations suggest that LAGO is vulnerable when text-side

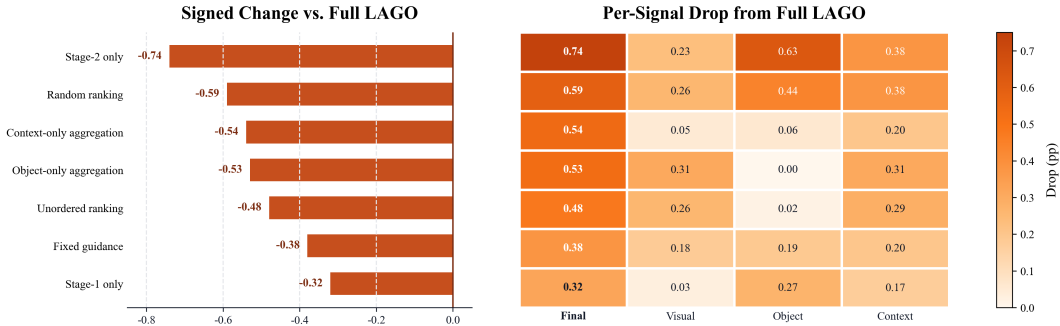


Figure 5: **Component ablations of LAGO.** Ablation results showing improved prediction quality through region discovery and refinement. Values denote gains of Full LAGO over each variant.

cues are misleading, when proposals fail to isolate the discriminative region, or when competing categories share similar attributes even after refinement. Examples are provided in Appendix C.4.

4.4 Component Ablations

We ablate LAGO’s components to verify its localized alignment strategy. These ablations test four questions: the need for class-agnostic initialization before semantic refinement, the benefit of confidence-aware guidance in avoiding the *prediction loop*, the value of ranked over random or unordered region selection, and the contribution of object-context aggregation beyond object crops.

Effect of the two-stage design. As shown in Figure 5, Full LAGO improves over Stage 1 only and Stage 2 only by **0.32%** and **0.74%**, respectively. Stage 1 only removes text-guided refinement, showing that visual-only localization is insufficient. Stage 2 only removes class-agnostic initialization and applies semantic refinement from the start, causing a larger drop and exposing the *prediction loop* risk from unreliable early semantics. This supports establishing stable visual initialization before introducing semantic guidance. Representative Stage 2-only failures are provided in Appendix D.

Effect of confidence-aware region discovery. Replacing confidence-aware guidance with fixed semantic guidance leads to a **0.38%** drop. This variant keeps semantic refinement but removes sample-specific confidence control, allowing unreliable early predictions to influence localization too strongly and amplify errors. In contrast, confidence-aware guidance weakens semantic focusing for uncertain samples and applies stronger refinement only when the intermediate prediction is more reliable. Full LAGO also improves over random and unordered region selection by **0.59%** and **0.48%**, respectively. These results show that LAGO benefits from selecting informative regions rather than merely using candidate crops. This supports our efficiency analysis: compact region discovery works because selected regions provide stronger, more reliable evidence than random or redundant crops.

Effect of object-context aggregation. Removing either channel degrades performance, with Full LAGO improving over object-only and context-only variants by **0.53%** and **0.54%**, respectively. This confirms that object-focused regions and contextual evidence provide complementary information across different object scales and layouts. The result supports our design choice to combine object, context, and full-image evidence, especially when local object cues are incomplete or ambiguous.

5 Conclusion

We presented LAGO, a language-guided adaptive localization framework for zero-shot visual-text alignment. Our results show that, in description-based zero-shot recognition, improving region discovery is as important as enriching class semantics. By combining object-centric initialization, confidence-aware two-stage refinement, and object-context aggregation, LAGO improves both accuracy and inference efficiency over prior localized alignment methods. These results suggest that selective, adaptive region-level alignment is more effective than exhaustive crop enumeration.

Limitations. LAGO still depends on the quality of external proposals and offline text descriptions, and its multi-stage inference pipeline remains more complex than single-pass global alignment. Future work may focus on stronger proposal generation, more robust text prototype construction, and simpler, leaner or more integrated inference schemes for multi-stage localization and refinement.

References

- [1] Alec Radford, Jong Wook Kim, Chris Hallacy, Aditya Ramesh, Gabriel Goh, Sandhini Agarwal, Girish Sastry, Amanda Askell, Pamela Mishkin, Jack Clark, Gretchen Krueger, and Ilya Sutskever. Learning transferable visual models from natural language supervision. In *Proceedings of the 38th International Conference on Machine Learning*, 2021.
- [2] Kaiyang Zhou, Jingkang Yang, Chen Change Loy, and Ziwei Liu. Learning to prompt for vision-language models. *International Journal of Computer Vision*, 2022.
- [3] Kaiyang Zhou, Jingkang Yang, Chen Change Loy, and Ziwei Liu. Conditional prompt learning for vision-language models. In *Proceedings of the IEEE/CVF Conference on Computer Vision and Pattern Recognition*, 2022.
- [4] Sachit Menon and Carl Vondrick. Visual classification via description from large language models. In *International Conference on Learning Representations*, 2022.
- [5] Sarah Pratt, Ian Covert, Rosanne Liu, and Ali Farhadi. What does a platypus look like? generating customized prompts for zero-shot image classification. In *Proceedings of the IEEE/CVF International Conference on Computer Vision*, pages 15691–15701, 2023.
- [6] Jinhao Li, Haopeng Li, Sarah Erfani, Lei Feng, James Bailey, and Feng Liu. Visual-text cross alignment: Refining the similarity score in vision-language models. In *Proceedings of the 41st International Conference on Machine Learning*, 2024.
- [7] Karsten Roth, Jae Myung Kim, A. Sophia Koepke, Oriol Vinyals, Cordelia Schmid, and Zeynep Akata. Waffling around for performance: Visual classification with random words and broad concepts. In *Proceedings of the IEEE/CVF International Conference on Computer Vision*, 2023.
- [8] Yuhao Sun, Chengyi Cai, Jiacheng Zhang, Zesheng Ye, Xingliang Yuan, and Feng Liu. Let's roll a bifta: Bi-refinement for fine-grained text-visual alignment in vision-language models. *Transactions on Machine Learning Research*, 2026.
- [9] Chunyu Xie, Bin Wang, Fanjing Kong, Jincheng Li, Dawei Liang, Gengshen Zhang, Dawei Leng, and Yuhui Yin. FG-CLIP: Fine-grained visual and textual alignment. *arXiv preprint arXiv:2505.05071*, 2025.
- [10] Lincan Cai, Jingxuan Kang, Shuang Li, Wenxuan Ma, Binhui Xie, Zhida Qin, and Jian Liang. From local details to global context: Advancing vision-language models with attention-based selection. In *Proceedings of the 42nd International Conference on Machine Learning (ICML 2025)*, volume 267 of *Proceedings of Machine Learning Research*, pages 6229–6242. PMLR, 2025.
- [11] Yuhang Zang, Wei Li, Kaiyang Zhou, Chen Huang, and Chen Change Loy. Unified vision and language prompt learning. *arXiv preprint arXiv:2210.07225*, 2022.
- [12] Yu Lu, Xiao Liu, Yuxin Zhang, Xiao Liu, and Xinmei Tian. Prompt distribution learning. In *Proceedings of the IEEE/CVF Conference on Computer Vision and Pattern Recognition*, pages 5206–5215, 2022.
- [13] Beier Zhu, Yulei Niu, Yucheng Han, Yue Wu, and Hanwang Zhang. Prompt-aligned gradient for prompt tuning. In *Proceedings of the IEEE/CVF International Conference on Computer Vision*, pages 15659–15669, 2023.
- [14] Hantao Yao, Rui Zhang, and Changsheng Xu. Visual-language prompt tuning with knowledge-guided context optimization. In *Proceedings of the IEEE/CVF Conference on Computer Vision and Pattern Recognition*, pages 6757–6767, 2023.
- [15] Muhammad Uzair Khattak, Hanoona Rasheed, Muhammad Maaz, Salman Khan, and Fahad Shahbaz Khan. Maple: Multi-modal prompt learning. *arXiv preprint arXiv:2210.03117*, 2023.
- [16] Muhammad Uzair Khattak, Hanoona Rasheed, Muhammad Maaz, Salman Khan, and Fahad Shahbaz Khan. Self-regulating prompts: Foundational model adaptation without forgetting. In *Proceedings of the IEEE/CVF International Conference on Computer Vision*, 2023.

- [17] Hongming Yao, Aixi Zhang, Xiaoshan Xu, Sicong Liu, Saining Xie, and Qingming Lu. TcP: Textual-based class-aware prompt tuning for visual-language model. In *Proceedings of the IEEE/CVF Conference on Computer Vision and Pattern Recognition*, 2024.
- [18] Muhammad Uzair Khattak, Muhammad Ferjad Naeem, Muzammal Naseer, Luc Van Gool, and Federico Tombari. Learning to prompt with text only supervision for vision-language models. *arXiv preprint arXiv:2401.02418*, 2024.
- [19] Hong-You Chen, Zhengfeng Lai, Haotian Zhang, Xinze Wang, Marcin Eichner, Keen You, Meng Cao, Bowen Zhang, Yinfei Yang, and Zhe Gan. Contrastive localized language-image pre-training. In *Proceedings of the 42nd International Conference on Machine Learning (ICML 2025)*, volume 267 of *Proceedings of Machine Learning Research*, pages 8386–8402. PMLR, 2025.
- [20] Rui Xiao, Sanghwan Kim, Mariana-Iuliana Georgescu, Zeynep Akata, and Stephan Alaniz. Flair: Vlm with fine-grained language-informed image representations. In *Proceedings of the IEEE/CVF Conference on Computer Vision and Pattern Recognition (CVPR 2025)*, pages 24884–24894, 2025.
- [21] Manli Shu, Weili Nie, De-An Huang, Zhiding Yu, Tom Goldstein, Anima Anandkumar, and Chaowei Xiao. Test-time prompt tuning for zero-shot generalization in vision-language models. In *Advances in Neural Information Processing Systems*, 2022.
- [22] Chun-Mei Feng, Kai Yu, Yong Liu, Salman Khan, and Wangmeng Zuo. Diverse data augmentation with diffusions for effective test-time prompt tuning. In *Proceedings of the IEEE/CVF International Conference on Computer Vision*, 2023.
- [23] Hee Suk Yoon, Eunseop Yoon, Joshua Tian Jin Tee, Mark A. Hasegawa-Johnson, Yingzhen Li, and Chang D. Yoo. C-TPT: Calibrated test-time prompt tuning for vision-language models via text feature dispersion. In *The Twelfth International Conference on Learning Representations*, 2024. URL <https://openreview.net/forum?id=jzzEHTBFOT>.
- [24] Jameel Hassan Abdul Samadh, Hanan Gani, Noor Hazim Hussein, Muhammad Uzair Khattak, Muzammal Naseer, Salman Khan, and Fahad Shahbaz Khan. Align your prompts: Test-time prompting with distribution alignment for zero-shot generalization. In *Advances in Neural Information Processing Systems*, 2023.
- [25] Gustavo Adolfo Vargas Hakim, David Osowiechi, Mehrdad Noori, Milad Cheraghlikhani, Ali Bahri, Moslem Yazdanpanah, Ismail Ben Ayed, and Christian Desrosiers. Clipartt: Adaptation of clip to new domains at test time. In *Proceedings of the IEEE/CVF Winter Conference on Applications of Computer Vision*, 2025.
- [26] Max Zanella, Ismail Ben Ayed, and Jose Dolz. On the test-time zero-shot generalization of vision-language models: Do we really need prompt learning? In *Proceedings of the IEEE/CVF Conference on Computer Vision and Pattern Recognition*, 2024.
- [27] Eric Arazo, Diego Ortego, Paul Albert, Noel E. O’Connor, and Kevin McGuinness. Pseudo-labeling and confirmation bias in deep semi-supervised learning. In *Proceedings of the 2020 International Joint Conference on Neural Networks (IJCNN)*, pages 1–8. IEEE, 2020.
- [28] Baixu Chen, Junguang Jiang, Ximei Wang, Pengfei Wan, Jianmin Wang, and Mingsheng Long. Debiased self-training for semi-supervised learning. In *Advances in Neural Information Processing Systems*, volume 35, pages 32424–32437, 2022.
- [29] Shilong Liu, Zhaoyang Zeng, Tianhe Ren, Feng Li, Hao Zhang, Jie Yang, Qing Jiang, Chunyuan Li, Jianwei Yang, Hang Su, Jun Zhu, and Lei Zhang. Grounding dino: Marrying dino with grounded pre-training for open-set object detection. *arXiv preprint arXiv:2303.05499*, 2023.
- [30] Linhui Xiao, Xiaoshan Yang, Xiangyuan Lan, Yaowei Wang, and Changsheng Xu. Towards visual grounding: A survey. *arXiv preprint arXiv:2412.20206*, 2024.
- [31] Penghao Wu and Saining Xie. V*: Guided visual search as a core mechanism in multimodal llms. In *Proceedings of the IEEE/CVF Conference on Computer Vision and Pattern Recognition*, 2024.
- [32] Qiji Zhou, Ruochen Zhou, Zike Hu, Panzhong Lu, Siyang Gao, and Yue Zhang. Image-of-thought prompting for visual reasoning refinement in multimodal large language models. *arXiv preprint arXiv:2405.13872*, 2024.
- [33] Xintong Zhang, Zhi Gao, Bofei Zhang, Pengxiang Li, Xiaowen Zhang, Yang Liu, Tao Yuan, Yuwei Wu, Yunde Jia, Song-Chun Zhu, and Qing Li. Chain-of-focus: Adaptive visual search and zooming for multimodal reasoning via rl. *arXiv preprint arXiv:2505.15436*, 2025.

- [34] Jiacong Wang, Zijiang Kang, Haochen Wang, Haiyong Jiang, Jiawen Li, Bohong Wu, Ya Wang, Jiao Ran, Xiao Liang, Chao Feng, and Jun Xiao. Vgr: Visual grounded reasoning. *arXiv preprint arXiv:2506.11991*, 2025.
- [35] Licheng Yu, Zhe Lin, Xiaohui Shen, Jimei Yang, Xin Lu, Mohit Bansal, and Tamara L. Berg. Mattnet: Modular attention network for referring expression comprehension. In *Proceedings of the IEEE/CVF Conference on Computer Vision and Pattern Recognition*, 2018.
- [36] Jiajun Deng, Zhengyuan Yang, Tianlang Chen, Wengang Zhou, and Houqiang Li. Transvg: End-to-end visual grounding with transformers. In *Proceedings of the IEEE/CVF International Conference on Computer Vision*, 2021.
- [37] Liunian Harold Li, Pengchuan Zhang, Haotian Zhang, Jianwei Yang, Chunyuan Li, Yiwu Zhong, Lijuan Wang, Lu Yuan, Lei Zhang, Jenq-Neng Hwang, Kai-Wei Chang, and Jianfeng Gao. Grounded language-image pre-training. In *Proceedings of the IEEE/CVF Conference on Computer Vision and Pattern Recognition*, 2022.
- [38] Seonghoon Yu, Paul Hongsuck Seo, and Jeany Son. Zero-shot referring image segmentation with global-local context features. In *Proceedings of the IEEE/CVF Conference on Computer Vision and Pattern Recognition (CVPR 2023)*, pages 19456–19465, 2023.
- [39] Ziqin Zhou, Yinjie Lei, Bowen Zhang, Lingqiao Liu, and Yifan Liu. Zegclip: Towards adapting clip for zero-shot semantic segmentation. In *Proceedings of the IEEE/CVF Conference on Computer Vision and Pattern Recognition (CVPR 2023)*, pages 11175–11185, 2023.
- [40] Xu Zhao, Wenchao Ding, Yongqi An, Yinglong Du, Tao Yu, Min Li, Ming Tang, and Jinqiao Wang. Fast segment anything. *arXiv preprint arXiv:2306.12156*, 2023.
- [41] C. Lawrence Zitnick and Piotr Dollár. Edge boxes: Locating object proposals from edges. In *Proceedings of the European Conference on Computer Vision (ECCV)*, pages 391–405, Cham, September 2014. Springer International Publishing.
- [42] Jia Deng, Wei Dong, Richard Socher, Li-Jia Li, Kai Li, and Li Fei-Fei. Imagenet: A large-scale hierarchical image database. In *Proceedings of the IEEE Conference on Computer Vision and Pattern Recognition*, pages 248–255, 2009.
- [43] Peter Welinder, Steve Branson, Takeo Mita, Catherine Wah, Florian Schroff, Serge Belongie, and Pietro Perona. Caltech-ucsd birds 200. Technical Report CNS-TR-2010-001, California Institute of Technology, 2010.
- [44] Omkar M. Parkhi, Andrea Vedaldi, Andrew Zisserman, and C. V. Jawahar. Cats and dogs. In *Proceedings of the IEEE Conference on Computer Vision and Pattern Recognition*, pages 3498–3505, 2012.
- [45] Mircea Cimpoi, Subhansu Maji, Iasonas Kokkinos, Sami Mohamed, and Andrea Vedaldi. Describing textures in the wild. In *Proceedings of the IEEE Conference on Computer Vision and Pattern Recognition*, pages 3606–3613, 2014.
- [46] Lukas Bossard, Matthieu Guillaumin, and Luc Van Gool. Food-101 – mining discriminative components with random forests. In *European Conference on Computer Vision*, pages 446–461, 2014.
- [47] Bolei Zhou, Agata Lapedriza, Aditya Khosla, Aude Oliva, and Antonio Torralba. Places: A 10 million image database for scene recognition. *IEEE Transactions on Pattern Analysis and Machine Intelligence*, 40(6):1452–1464, 2018.
- [48] Benjamin Recht, Rebecca Roelofs, Ludwig Schmidt, and Vaishal Shankar. Do imagenet classifiers generalize to imagenet? In *Proceedings of the 36th International Conference on Machine Learning*, pages 5389–5400, 2019.
- [49] Dan Hendrycks, Steven Basart, Norman Mu, Sanjay Kadavath, Frank Wang, Evan Dorundo, Rahul Desai, Tyler Zhu, Samyak Parajuli, Mike Guo, Dawn Song, Jacob Steinhardt, and Justin Gilmer. The many faces of robustness: A critical analysis of out-of-distribution generalization. In *Proceedings of the IEEE/CVF International Conference on Computer Vision*, pages 8340–8349, 2021.
- [50] Haohan Wang, Songwei Ge, Zachary Lipton, and Eric P. Xing. Learning robust global representations by penalizing local predictive power. In *Advances in Neural Information Processing Systems*, volume 32, 2019.
- [51] Dan Hendrycks, Kevin Zhao, Steven Basart, Jacob Steinhardt, and Dawn Song. Natural adversarial examples. In *Proceedings of the IEEE/CVF Conference on Computer Vision and Pattern Recognition*, pages 15262–15271, 2021.

A Additional Method Details

A.1 Offline Text Construction and Text Prototype Formation

Following prior description-based zero-shot works [4, 5], and adopting a lightweight text-side refinement strategy similar to BiFTA [8], we maintain an offline curated class-specific semantic description set for each class $y \in \mathcal{Y}$ that serves as stable text supervision during inference:

$$\mathcal{T}^{(y)} = \{T_1^{(y)}, T_2^{(y)}, \dots, T_m^{(y)}\}, \quad (14)$$

where each sentence describes fine-grained semantic properties such as parts, attributes, textures, or contextual cues. Each sentence is encoded by the frozen text encoder of CLIP [1], and the resulting embeddings are aggregated into a class representation. By default, we simply use mean pooling:

$$\mathbf{t}_y = \frac{1}{m} \sum_{i=1}^m g(T_i^{(y)}). \quad (15)$$

Optionally, we apply a lightweight template-guided reweighting scheme. Let \hat{T}_y denote a canonical class template such as “a photo of a {class}”, and let $\mathbf{u}_y = g(\hat{T}_y)$. We compute sentence weights by

$$a_i^{(y)} = \frac{\exp(\tau \mathbf{u}_y^\top g(T_i^{(y)}))}{\sum_{j=1}^m \exp(\tau \mathbf{u}_y^\top g(T_j^{(y)}))}, \quad (16)$$

and obtain the class representation as a weighted sum over all encoded descriptions

$$\mathbf{t}_y = \sum_{i=1}^m a_i^{(y)} g(T_i^{(y)}), \quad (17)$$

where τ is a temperature parameter controlling the sharpness of the reweighting process.

During Stage 2, we construct an adaptive text prototype from the intermediate logits $\mathbf{z}^{(1)}$. Let

$$\pi_y = \frac{\exp(z_y^{(1)}/\tau_z)}{\sum_{y' \in \mathcal{Y}} \exp(z_{y'}^{(1)}/\tau_z)}, \quad (18)$$

where τ_z is a scalar temperature parameter. The Stage 2 text prototype is then computed

$$\mathbf{w}_{\text{text}} = \sum_{y \in \mathcal{Y}} \pi_y \mathbf{t}_y. \quad (19)$$

This prototype provides a soft semantic target that remains stable under uncertain intermediate confidence estimates for adaptive text-guided refinement without committing to a single early prediction.

A.2 Detailed Proposal-Centered Search

This section provides the low-level practical implementation details of the proposal-centered search routine used in the confidence-aware two-stage region discovery procedure in Sec. 3.3. In our framework, this routine is not treated as a separate conceptual component, but as the underlying mechanism for efficiently constructing and refining object-centric crop candidates, in a manner broadly related to localized visual grounding and language-guided region reasoning [29, 35–37].

We formulate crop localization as a constrained search optimization problem over bounding boxes. Given an image, the goal is to find a box b that maximizes a stage-dependent scoring function:

$$b^* = \arg \max_b S(b), \quad (20)$$

where

$$S(b) = (1 - \gamma) S_{\text{visual}}(b) + \gamma S_{\text{text}}(b). \quad (21)$$

Here, $S_{\text{visual}}(b)$ measures the local visual quality or saliency of the crop, while $S_{\text{text}}(b)$ measures alignment with corresponding text features. The parameter γ controls the relative contribution of semantic guidance: in Stage 1, $\gamma = 0$ and the search is purely visual throughout this stage; in Stage 2, γ directly is determined adaptively from the intermediate confidence score for each sample.

Algorithm 2 summarizes the low-level proposal-centered search routine used by both stages.

Algorithm 2: Proposal-Centered SEARCHTOPKCROPS

Require: image x , initial box b_0 , full-image feature \mathbf{v}_{full} , optional target text feature \mathbf{w}_{tgt} , guidance weight γ

Ensure: top- K diverse crop set \mathcal{C}

```
1 Function SEARCHTOPKCROPS( $x, b_0, \mathbf{v}_{\text{full}}, \mathbf{w}_{\text{tgt}}, \gamma$ )
2    $b \leftarrow \text{CLAMP\_TO\_IMAGE}(b_0)$ 
3    $\mathcal{S} \leftarrow \emptyset$ 
4   foreach  $stage \in \{coarse, fine\}$  do
5     set stage-specific parameters ( $T, \delta, \rho$ )
6     for  $t \leftarrow 1$  to  $T$  do
7        $\mathcal{N} \leftarrow \text{GENERATE\_NEIGHBORS}(b, \delta, \rho)$ 
8       foreach  $b' \in \mathcal{N}$  do
9         compute  $S_{\text{visual}}(b')$ 
10        if  $\mathbf{w}_{\text{tgt}}$  is available then
11          compute  $S_{\text{text}}(b')$ 
12           $s(b') \leftarrow (1 - \gamma)S_{\text{visual}}(b') + \gamma S_{\text{text}}(b')$ 
13        else
14           $s(b') \leftarrow S_{\text{visual}}(b')$ 
15          add  $(b', s(b'))$  to  $\mathcal{S}$ 
16         $\hat{b} \leftarrow \arg \max_{b' \in \mathcal{N}} s(b')$ 
17        if  $s(\hat{b}) - s(b) < \epsilon$  then
18          break
19         $b \leftarrow \hat{b}$ 
20    $\mathcal{C} \leftarrow \text{DIVERSE\_TOPK}(\mathcal{S}, K, \tau_{\text{search}})$ 
21   return  $\mathcal{C}$ 
```

Multi-start greedy refinement. To solve the optimization efficiently, we adopt a multi-start greedy search initialized from proposal regions generated by FastSAM [40]. For each proposal box $b_m^{(0)} \in \mathcal{B}_0$, we iteratively refine its location by exploring local neighborhoods and moving toward higher-scoring candidates. Let b_t denote the current box at iteration t . At each step, we update the state by

$$b_{t+1} = \arg \max_{b' \in \mathcal{N}(b_t)} S(b'). \quad (22)$$

This process is repeated for a fixed number of steps T for each proposal box independently.

Neighborhood generation. Given a current box defined in image coordinate space,

$$b = (x, y, w, h), \quad (23)$$

we generate local neighboring boxes by applying spatial shifts and scale perturbations:

$$b' = (x + \Delta x, y + \Delta y, w(1 + \rho_w), h(1 + \rho_h)), \quad (24)$$

where Δx and Δy denote translation offsets, and ρ_w, ρ_h denote width and height scaling factors.

Coarse-to-fine search schedule. To balance exploration and stability, we employ a coarse-to-fine search schedule. Larger perturbations are used during early iterations to gradually explore a broader portion of the search space, whereas smaller perturbations are used later for local refinement.

IoU-diverse top- k selection. Each proposal-centered search trajectory produces a set of visited candidate boxes with associated scores at each iteration. Because neighboring search steps often yield highly overlapping and redundant boxes, we apply an IoU-based diversity filter before caching the search results. Candidates are first sorted by score in descending order, and then selected greedily under the diversity constraint. A candidate is retained only if its IoU with every previously selected box is below a threshold τ_{search} . This process continues until a diverse top- k subset is obtained.

Let the final cached proposal-guided crop set after diversity filtering for each image be

$$\mathcal{C}^{(0)} = \{c_1^{(0)}, c_2^{(0)}, \dots, c_K^{(0)}\}. \quad (25)$$

These cached crops are reused at inference time and serve as the object-centric initialization for subsequent region discovery and scoring for all later stages of confidence-aware semantic refinement.

Complexity. Let M denote the number of initial proposals, T the number of search steps per proposal, and $|\mathcal{N}|$ the neighborhood size. The offline search complexity under this setting is

$$\mathcal{O}(MT|\mathcal{N}|), \quad (26)$$

excluding feature evaluation cost. Since the resulting crops are cached, this cost is incurred only once during crop construction rather than during each test-time evaluation. By contrast, the dominant online cost of LAGO is proportional to the number of encoded views used at inference time.

A.3 Additional View Refinement

A major source of inefficiency in crop-based inference is redundancy: many crops are highly overlapping and provide nearly identical visual evidence across candidate views. In our implementation, we explicitly reduce this redundancy at two distinct stages of the pipeline for better overall efficiency.

IoU filtering for online random completion crops. At inference time, each image is represented by the full image, a set of cached proposal-guided crops, and, when necessary, additional random crops that fill the remaining slots up to a target number of views. Since these random completion crops may strongly overlap with existing views, we apply a greedy IoU filtering step only to them.

Let V denote the set of already accepted boxes, initialized with the full-image box and the cached proposal-guided boxes. For a newly sampled random crop candidate b_i , we keep it only if

$$f_{\text{rand}}(b_i, V) = \begin{cases} 1, & \forall b \in V, \text{IoU}(b, b_i) < \tau_{\text{rand}}, \\ 0, & \text{otherwise.} \end{cases} \quad (27)$$

If $f_{\text{rand}}(b_i, V) = 1$, we update $V \leftarrow V \cup b_i$; otherwise the crop is discarded. This step suppresses near-duplicate random context crops while always retaining the full image and the cached proposal-guided views for stable and efficient downstream dual-channel aggregation during inference.

Relation to offline diversity filtering. The IoU filtering above is distinct from the IoU-diverse top- k selection used during offline proposal-centered search. The former explicitly operates online on random completion crops to improve contextual diversity at inference time, whereas the latter operates offline on search trajectories to improve diversity among proposal-guided object candidates.

A.4 Fixed-Shape Crop Representation and Batched Inference

To enable efficient batched evaluation during inference while preserving balanced crop diversity overall, we represent each image using a fixed number of views. Specifically, each image includes:

1. the full image,
2. a set of cached proposal-guided crops,
3. optional random completion crops if the target number of views has not been reached.

If the number of valid crops is smaller than the fixed tensor length, we pad the remaining slots with zero crops and use a validity mask to exclude them from subsequent aggregation. This fixed-shape design significantly simplifies batching and implementation at inference time, while ensuring that invalid padded crops do not affect the final score or downstream prediction stability overall.

A.5 Dataset-Specific Score Calibration

The fusion weights $(\beta, \alpha_{\text{dc}}, \lambda)$ may vary across datasets and backbone configurations. To study this sensitivity, we optionally apply a lightweight score-level calibration procedure that selects these parameters by grid search on precomputed features. This procedure does not update any

Table 3: **Accuracy-oriented ablation studies of LAGO on ImageNet-V2.** We report final accuracy (%) along with visual, object, and context component accuracies under different architectural and inference design choices. The best-performing variant is highlighted for easier comparison.

Stage	Guidance	Ranking	Aggregation	Final Acc (%)	Visual Acc (%)	Object Acc (%)	Context Acc (%)
stage1 only	adaptive	ranked	dual	65.58	64.78	65.04	65.31
stage2 only	adaptive	ranked	dual	65.16	64.58	64.68	65.10
two stage	fixed	ranked	dual	65.52	64.63	65.12	65.28
two stage	adaptive	random	dual	65.31	64.55	64.87	65.10
two stage	adaptive	unordered	dual	65.42	64.55	65.29	65.19
two stage	adaptive	ranked	object-only	65.37	64.50	65.31	65.17
two stage	adaptive	ranked	context-only	65.36	64.76	65.25	65.28
two_stage	adaptive	ranked	dual	65.90	64.81	65.31	65.48

Table 4: **Candidate-region efficiency under fixed inference budgets on ImageNet-V2.** We vary the number of candidate regions used at inference and report top-1 accuracy (%) under different budgets.

Method	8	16	24	32	48	64
WCA	63.96	64.44	64.44	64.53	64.55	64.44
LAGO	63.48	64.49	64.88	65.06	65.33	65.56
Δ	-0.48	+0.05	+0.44	+0.53	+0.78	+1.12

model parameters, but it does constitute dataset-specific score calibration rather than strictly training-free zero-shot inference. We therefore treat it as an optional implementation variant and report it separately from the core training-free formulation of LAGO. Since the calibration operates only on frozen precomputed scores, it still introduces negligible additional computational overhead.

B Detailed Ablation Results

We provide the full numerical results for the ablation studies summarized in Figure 5 for completeness and detailed quantitative comparison overall. Table 3 reports the accuracy-oriented ablations.

Table 3 shows that the main accuracy gain primarily comes from the proposed confidence-aware two-stage region discovery. The full model achieves **65.90%**, consistently outperforming Stage 1 only (**65.58%**), Stage 2 only (**65.16%**), and the fixed-guidance variant (**65.52%**). These results indicate that semantic guidance is most effective when introduced only after a stable visual initialization has been fully established before refinement begins, and that adaptive confidence modulation further improves refinement in practice by reducing error amplification from unreliable early predictions.

The remaining design choices explain why LAGO is both compact and effective overall. Ranked candidates consistently outperform random (**65.31%**) and unordered (**65.42%**) selection, showing that the improvement comes from choosing better regions rather than simply processing more crops. Likewise, dual-channel aggregation outperforms object-only (**65.37%**) and context-only (**65.36%**) variants, confirming that contextual evidence meaningfully complements object-focused regions.

C Additional Analysis

C.1 Candidate-Region Efficiency

We further analyze whether LAGO uses a fixed candidate-region budget more effectively than WCA, where the budget denotes the total number of candidate regions evaluated per image at inference time. Table 4 shows that LAGO is slightly weaker at the smallest budget because too few regions leave limited room for proposal-centered search to establish sufficient coverage before refinement. As the budget increases, however, LAGO becomes consistently stronger than WCA, and the gap widens. This trend consistently supports our claim that LAGO gains not from exhaustive crop enumeration, but from increasingly informative and selective region discovery under a fixed inference budget.

C.2 Confidence-Aware Behavior

We provide additional analysis of the confidence-aware refinement mechanism. To understand where adaptive guidance is most beneficial, we group samples by their confidence and examine cases that are corrected by the adaptive variant but not by the fixed-guidance baseline at inference time.

Figure 7 (left) summarizes the distribution of such adaptive-corrected samples across confidence buckets overall in this analysis. We count cases that are corrected by adaptive guidance but not by the fixed-guidance variant at inference time. Most such corrections occur especially in the *low-confidence* regime, with a smaller but still meaningful number in the *medium-confidence* regime as well. This indicates that confidence-aware refinement is particularly helpful in practice under distribution shift when early predictions are unreliable at test time. The pattern is fully consistent with the motivation of LAGO: when intermediate predictions are uncertain, semantic guidance should be applied more cautiously and selectively in order to avoid error amplification from unreliable early predictions.

Figure 9 presents representative corrected cases. In these examples, the adaptive strategy consistently tends to preserve or recover semantically relevant evidence that would otherwise be overwhelmed by fixed guidance. Together, these results suggest that confidence is an effective sample-level signal for adaptively controlling how strongly textual information should influence region discovery.

C.3 Stage-wise Visualization

We provide additional qualitative examples to illustrate how region discovery evolves from Stage 1 to Stage 2. In all cases, Stage 1 performs visual-only localization and therefore tends to select visually salient, object-centric crops without assuming reliable class semantics. Stage 2 then progressively refines these regions with adaptive text guidance, shifting attention toward more semantically discriminative evidence associated with the predicted class. Together, these examples help visualize the role of the confidence-aware two-stage design: first stabilize localization, then refine it semantically.

Figure 6 highlights the refinement process in a single dataset with detailed per-example statistics, while Figure 8 shows that the same stage-wise behavior generalizes across multiple datasets.

C.4 Failure Analysis: ImageNet-R Case Study

We provide a qualitative failure analysis using ImageNet-R as a case study for zero-shot localized alignment analysis. We choose ImageNet-R because its artistic and stylized renditions, where appearance cues are often semantically misleading, make the alignment between class semantics and visually relevant regions particularly challenging under natural distribution shift at inference time.

Figure 7 (right) summarizes the qualitative distribution of failure categories in this analysis under natural distribution shift overall. The dominant failure mode is clearly *semantic mismatch*, followed by *cluttered or poorly localized regions*, *other* cases, and *visually ambiguous classes* at inference time. Figures 10–13 present representative examples of these categories for detailed qualitative inspection.

In this analysis, the largest category is *semantic mismatch* (**50.0%**), by a clear margin, where the text prototype often emphasizes cues that are weak, misleading, or absent in the image at inference time under distribution shift. The remaining failures are more evenly divided among *cluttered or poorly localized regions* (**21.4%**), *other* cases (**21.4%**), and *visually ambiguous classes* (**7.1%**).

Representative examples further illustrate these patterns. Semantic mismatch often occurs when the selected regions are locally plausible but semantically align with misleading text-side cues rather than the ground-truth class under distribution shift. Cluttered or poorly localized cases arise when the proposal set fails to fully isolate the truly discriminative content at inference time. Visually ambiguous cases remain difficult even after localized refinement because competing classes still share highly similar local attributes in practice. The remaining "other" cases include failures that do not fall cleanly into a single dominant category. Overall, these observations suggest that future improvements may come from stronger proposal generation quality and more robust text prototype construction.

D Stage 2-only Failure Cases

To further support the component ablation in Figure 5, we visualize two representative failure cases of the Stage 2-only variant. This variant removes class-agnostic visual initialization and applies

semantic refinement from the beginning. As a result, region selection can be influenced by unreliable early semantic estimates in zero-shot inference before stable object-centric candidates are established.

As shown in Figures 14 and 15, Stage 2-only refinement does not reliably separate the ground-truth class from visually or semantically related alternatives. These examples illustrate the *prediction loop*: uncertain early predictions guide region selection, and the resulting regions further reinforce incorrect or ambiguous predictions. Full LAGO mitigates this issue by first discovering stable and reliable class-agnostic object-centric candidates and then applying confidence-aware text-guided refinement.

E Additional Qualitative Analysis of Crop Reweighting

We provide additional qualitative examples to illustrate how LAGO reweights crop-level evidence at inference time. Rather than modifying the text encoder itself, LAGO refines prediction by assigning higher weights to crops that provide more reliable, semantically discriminative object-level evidence and suppressing crops that are less informative, ambiguous, or dominated by background or context.

In each example, the top-left panel shows the original test image, and the top-right panel compares the prediction distribution before and after applying LAGO at inference time over a focused set of candidate classes. The bottom-left panel shows the prediction distributions of crops assigned relatively low weights by LAGO, while the bottom-right panel shows the distributions of the top LAGO-weighted crops. For readability, the ridge plots are shown over a visually interpretable focused subset of classes, and the red dashed line marks the ground-truth class. The visualization temperature and candidate subset are strictly used only for display and do not affect the model’s final prediction.

Across datasets, a consistent pattern emerges. LAGO tends to suppress noisy or weakly relevant crops, such as background-dominated views or crops whose evidence is semantically diffuse, while emphasizing crops whose evidence is more visually and semantically concentrated around the target object. As a result, the weighted crop evidence becomes more aligned with the ground-truth class after aggregation, illustrating how the proposed crop reweighting mechanism improves localized visual-text alignment overall. Representative examples on Oxford Pets are shown in Figures 16–18, while Figures 19–21 illustrate the same behavior on Food101, ImageNet-V2, and ImageNet-R.

F Additional Human Evaluation Analysis

We provide an additional human evaluation to directly examine whether the region paths discovered by LAGO align more closely with human-perceived discriminative evidence at inference time under a natural distribution shift. This analysis complements the accuracy results in the main paper: instead of only measuring whether the final predicted label is correct, it evaluates whether the selected regions correspond to visual evidence that humans consider useful for recognizing the ground-truth class in practice. The evaluation is used only for analysis and is not used to tune the method in any form.

We conduct the study on 100 selected samples spanning five diverse datasets: CUB, Oxford Pets, ImageNet, DTD, and ImageNet-R. Four independent evaluators annotate the same questionnaire. For each image, the evaluators are shown the original image, the ground-truth class label, and two candidate region sets generated by Stage 1 and Stage 2, presented as anonymized options. They are asked to answer two questions: (1) which option better supports recognizing the ground-truth category, and (2) whether the Stage 2 regions capture the key visual evidence needed for recognition.

Evaluation protocol. The first question provides a *more direct* relative comparison between Stage 1 and Stage 2: *Which region set better supports recognizing the ground-truth class?* The displayed answer is one of the two anonymized options or a tie. After unblinding with the hidden option mapping, we convert each response to one of Stage1, Stage2, Tie for later quantitative analysis. This relative comparison is designed to more clearly test whether the adaptive semantic refinement in Stage 2 indeed improves over the visual-only localization in Stage 1 from a human perspective.

The second question provides an *absolute* human judgment of Stage 2: *Do the Stage 2 regions capture the key visual evidence needed to recognize the ground-truth class?* The answer is one of Yes, Partially, No. We report both a strict binary alignment rate, where only Yes is counted as aligned, and a soft partial-credit score, where Yes/Partially/No are mapped to 1/0.5/0, respectively.

Table 5: **Overall human evaluation results.** Stage 2 is consistently favored overall in the relative comparison, especially after excluding ties, under the human evaluation protocol used in this study, while its absolute alignment score remains positive and varies across evaluators in practice.

Scope	Answered	Stage 2 Pref.	Pref. (w/o Ties)	Strict Align.	Partial Score
Evaluator A	100	82.0%	83.7%	74.0%	0.865
Evaluator B	100	70.0%	89.7%	48.0%	0.585
Evaluator C	100	65.0%	77.4%	59.0%	0.715
Evaluator D	100	46.0%	59.0%	82.0%	0.900
Pooled	400	65.8%	77.8%	65.8%	0.766

F.1 Overall Results

Table 5 summarizes the overall results from human evaluation under this protocol. Across the four evaluators, Stage 2 is preferred in 263/400 responses (65.8%), and the preference further increases to 263/338 (77.8%) when ties are excluded. The fourth evaluator is more conservative in the relative Stage 1-versus-Stage 2 comparison, preferring Stage 2 in 46/100 responses (46.0%), or 46/78 (59.0%) after excluding ties. Even with this more conservative annotator included, the pooled non-tie preference remains clearly in favor of Stage 2. At the item level, all four evaluators prefer Stage 2 on 32/100 samples, a strict majority prefer Stage 2 on 57/100 samples, at least half prefer Stage 2 on 78/100 samples, and at least one evaluator prefers Stage 2 on 96/100 samples. Comparing Stage 2 votes directly against Stage 1 votes per sample, Stage 2 receives more votes on 75/100 samples, the two stages are tied on 13/100, and Stage 1 receives more votes on only 12/100. These results support the intended role of the confidence-aware refinement stage: after a stable visual initialization, Stage 2 tends to select region paths that humans judge as more useful and reliable under realistic recognition settings, while the exact relative preference remains evaluator-dependent on some ambiguous cases.

For the absolute judgment of Stage 2, the pooled strict alignment rate is 263/400 (65.8%), with a partial-credit mean of 0.766 across the four human evaluators in this study overall. The fourth evaluator gives a high absolute alignment score (82.0% strict alignment and 0.900 partial credit), which further strengthens the evidence that Stage 2 regions frequently capture useful visual evidence at inference time, even when the relative pairwise choice between Stage 1 and Stage 2 is more conservative. Thus, Stage 2 regions are frequently judged as plausible and informative under this protocol, although the absolute alignment judgment is still subjective and evaluator-dependent.

F.2 Agreement Between Evaluators

We further examine inter-rater agreement overall using Fleiss’ κ across the four evaluators in this setting, but interpret these statistics cautiously. For Question 1, the mean per-item observed agreement over the 100 samples with complete annotations is 0.627. On the anonymized option labels (A/B/Tie), this corresponds to Fleiss’ $\kappa = 0.390$. After mapping responses to the semantic labels (Stage1, Stage2, Tie), the observed agreement remains 0.627, but κ drops to 0.266 because the marginal distributions are skewed toward Stage 2. The pairwise Cohen’s κ values for this semantic preference range from 0.046 to 0.434 across evaluator pairs. These agreement statistics should therefore not be interpreted as evidence of strong item-level consensus about exactly which samples are improved by Stage 2. Instead, they indicate that the evaluators show an overall consistent directional preference for Stage 2, while differing on the particular cases for which that preference is expressed.

Agreement is also limited overall for the absolute Stage 2 alignment judgment for this question across all four evaluators in total: the three-way label (Yes/Partially/No) yields Fleiss’ $\kappa = 0.108$, and the strict binary alignment label yields $\kappa = 0.160$. This is still consistent with the evaluation design under this protocol, since the absolute adequacy of a single discovered region path is inherently much more subjective than a relative comparison between two alternatives. Overall, we treat the human evaluation as supportive but exploratory evidence in this study: it suggests, as observed here, a broad preference for Stage 2 over Stage 1 and frequent absolute Stage 2 alignment, but it should not be interpreted as strong evidence of high inter-rater reliability at the sample level in practice.

F.3 Dataset-wise Trends

Figures 22 and 23 break down the human evaluation results by dataset. The preference for Stage 2 is strongest on ImageNet-R and Oxford Pets, where Stage 2 is preferred in 78.8% and 77.2% of responses, respectively, followed by ImageNet (67.5%) and CUB (61.3%). This trend is consistent with the motivation of LAGO: semantic refinement is especially useful when localized visual evidence is important, or when distribution shift makes global image-level evidence less reliable at inference time. DTD is tie-heavy: Stage 2 is selected in 26/68 responses (38.2%) when ties are included, but in 26/30 non-tie responses (86.7%) when ties are excluded. This suggests that DTD often makes the relative comparison less clear-cut, rather than providing strong evidence against Stage 2 in practice.

A similar but not identical trend is also observed for strict alignment overall. Stage 2 achieves the highest strict alignment rate on CUB (83.8%), followed by DTD (72.1%), ImageNet-R (63.7%), ImageNet (57.5%), and Oxford Pets (54.3%). This suggests that the proposed region refinement is particularly effective on fine-grained bird recognition and remains useful, even under the stricter absolute alignment criterion, on texture- or distribution-shift-heavy cases, while absolute path quality remains more evaluator-dependent on visually diffuse or ambiguous categories in practice overall.

F.4 Relation to Prediction Correctness

We also analyze whether human-perceived path quality simply tracks final prediction correctness. In this selected subset, it does not. Under the pooled strict criterion, the alignment rate is $184/284 = 64.8\%$ on correctly predicted samples, but $79/116 = 68.1\%$ on incorrectly predicted samples. The partial-credit score shows a similar pattern (0.764 for correct predictions and 0.772 for incorrect predictions). This observation should not be interpreted as a causal negative correlation, since the subset composition and dataset difficulty may influence these counts. Instead, it indicates that path plausibility and final decision correctness capture different aspects of the recognition pipeline.

Figures 24 and 25 summarize the item-level Stage 2 preference consensus and the alignment distribution conditioned on prediction correctness overall. The result suggests that LAGO can often localize regions that appear semantically meaningful to humans at inference time even when the classification remains incorrect. This supports an important point in our analysis: residual errors do not always originate from region discovery itself in such cases. Some failures may instead arise from fine-grained semantic ambiguity, text-side mismatch, or downstream score aggregation after a visually plausible region has already been selected by the model for the final aggregated prediction.

F.5 Qualitative Implications

Figure 26 shows representative examples from the human evaluation across datasets. The qualitative cases illustrate the same two main conclusions as the quantitative results. First, Stage 2 often produces more semantically focused, discriminative, and visually grounded region sets than Stage 1, consistent with its strong non-tie human preference rate and majority item-level support. Second, a visually plausible Stage 2 path does not always imply a correct final prediction at inference time, especially in fine-grained recognition where nearby categories can still share highly similar local evidence.

Overall, under this protocol, the human evaluation provides additional qualitative evidence for the main design of LAGO. Stage 2 is consistently favored over Stage 1 overall, especially after excluding ties, supporting the role of sample-specific adaptive semantic refinement in region discovery at inference time across diverse datasets. At the same time, human-aligned paths do not always reliably lead to fully correct final predictions by themselves in practice, highlighting the distinction between *path plausibility* and *decision correctness*. This distinction is especially relevant in fine-grained recognition, where a region may often capture a visually meaningful attribute while still being insufficient to fully resolve subtle semantic differences between nearby categories in practice.

F.6 Participant Instructions and Compensation

The human evaluation was conducted as an offline annotation study using static visual questionnaires. Each questionnaire item contained the original image, the ground-truth class label, and two anonymized candidate region sets corresponding to Stage 1 and Stage 2, shown as Option A and Option B in randomized order. Evaluators were not told which option corresponded to which

stage during annotation. The evaluation was used only for qualitative and quantitative analysis of region-path plausibility and was not used for model selection, hyperparameter tuning, or training.

The full participant-facing instruction text was as follows:

You will be shown an image, its ground-truth class label, and two anonymized sets of candidate regions. Please judge the region sets based on whether they contain visual evidence useful for recognizing the ground-truth class. Do not infer which method produced each option. For each sample, answer the following two questions.

Question 1: Which region set better supports recognizing the ground-truth class? Please choose one of: Option A, Option B, or Tie.

Question 2: Do the Stage 2 regions capture the key visual evidence needed to recognize the ground-truth class? Please choose one of: Yes, Partially, or No.

For Question 1, the mapping between Option A/Option B and Stage 1/Stage 2 was hidden from evaluators and was used only after annotation for analysis. For Question 2, evaluators were shown the Stage 2 region set and asked to judge its absolute adequacy for recognizing the ground-truth class. No additional personal information was collected from the evaluators. The questionnaire consisted only of static images, class labels, candidate region visualizations, and multiple-choice responses.

No crowdsourcing platform was used. The four evaluators participated in an internal offline evaluation and completed the same questionnaire independently. No monetary compensation was provided for this exploratory analysis, which was voluntary and low burden. Since the study involved only non-sensitive visual judgments over public benchmark images and did not collect personal or behavioral data beyond annotation choices, we consider the overall risk to participants to be minimal.

F.7 Participant Risk Disclosure and Ethics Review

The human evaluation involved only non-sensitive visual judgments over public benchmark images. Evaluators were informed that the study was used to assess whether candidate region sets provide useful visual evidence for recognizing the provided ground-truth class label. The study did not involve deception, intervention, collection of personal information, or collection of behavioral data beyond multiple-choice annotation responses. The expected risk to participants was therefore minimal.

Under the applicable institutional policy, this exploratory internal annotation study did not require formal IRB approval or equivalent ethics-board review, because it involved minimal-risk non-sensitive visual judgments. Participation was voluntary, and evaluators could stop the annotation at any time. No identifying information about the evaluators is included in the paper or supplemental material.

G Additional Discussion

The main takeaway of this work is that the bottleneck in description-based zero-shot recognition lies not only in enriching class semantics, but also in aligning those semantics with the correct visual regions during inference. This distinction is important in practice: once class descriptions become sufficiently informative, performance is no longer determined solely by the quality of the text side, but increasingly by whether the model can identify the visual evidence that actually supports those semantics. From this perspective, zero-shot recognition is not simply a problem of semantic representation, but also a problem of selective, reliable, and robust evidence allocation.

Our results suggest that simply increasing the number of candidate crops is not the most effective way to address this challenge. Although large candidate sets improve coverage, they also introduce substantial redundancy and make the inference process more vulnerable to noisy or weakly relevant regions. In contrast, better region discovery plays a truly more central role. Class-agnostic object-centric initialization provides a stable visual starting point before uncertain class information is introduced; confidence-aware two-stage refinement controls when and how semantic guidance should influence localization; and object-context aggregation improves robustness when local evidence alone is incomplete or ambiguous. Taken together, these components indicate that the key issue is not how to enumerate more regions, but how to identify, selectively refine, and reliably use the right ones.

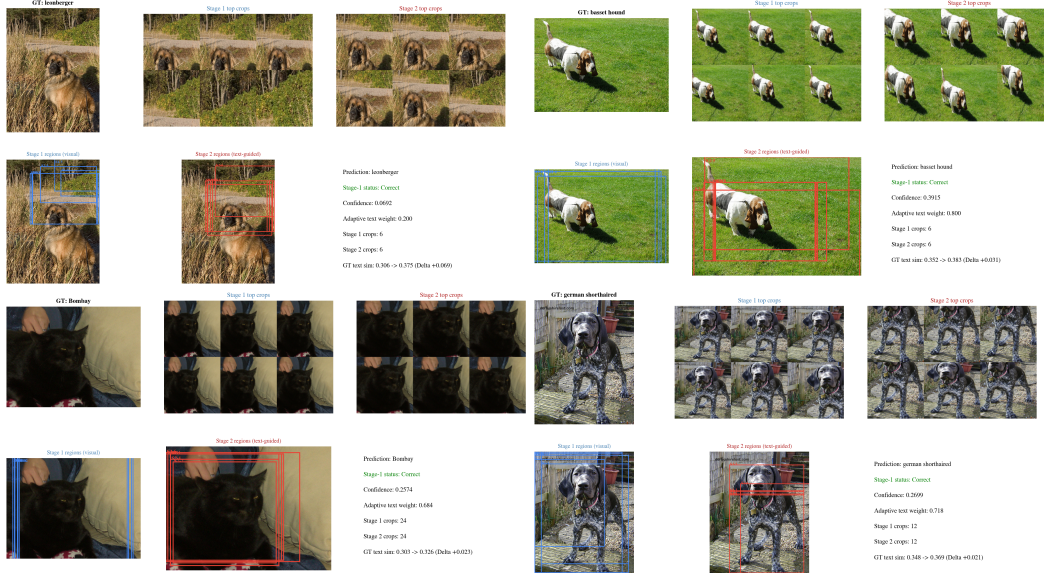


Figure 6: **Stage-wise visualization on Oxford Pets.** Each example shows the image, top crops from Stage 1 and Stage 2, their candidate regions, and statistics for confidence and text-similarity changes. Stage 1 selects object-centric regions, while Stage 2 further refines them toward more semantically informative, class-relevant evidence, increasing alignment with the ground-truth text prototype.

More broadly, these findings point to a useful view of localized zero-shot recognition: semantic guidance is most effective when it is introduced selectively and progressively, rather than applied uniformly from the outset. In this sense, the main challenge is not only to make localization semantic, but to make it reliable under uncertainty and robust to early prediction errors. This also more generally helps explain why the gains of LAGO are especially visible in fine-grained and distribution-shift settings, where discriminative evidence is localized, subtle, and easily confounded by early prediction errors in complex scenes. Overall, our results support the view that effective localized visual-text alignment should be adaptive, confidence-aware, and evidence-selective, rather than exhaustive.

H Broader Impacts

LAGO aims to improve zero-shot visual recognition by making visual-text alignment more localized, selective, and efficient. Potential positive impacts include reducing the need for task-specific labeled data, improving recognition robustness under distribution shifts, and lowering inference redundancy compared with exhaustive crop-based localized alignment methods. These properties may make vision-language recognition systems more practical in settings where annotation is expensive or where models must generalize to previously unseen categories across real-world application scenarios.

At the same time, improved zero-shot recognition can also introduce potential negative impacts, especially when adopted without governance and auditing. More accurate and efficient visual recognition systems may be used in surveillance, profiling, or other applications where individuals or groups could be monitored without appropriate consent. Because LAGO relies on pretrained vision-language models and offline text descriptions, it may also inherit biases from the underlying model, datasets, or textual descriptions, potentially leading to uneven performance across visual domains, object categories, cultural contexts, or demographic groups when deployed in settings.

The method is intended as a research contribution for evaluating and improving localized visual-text alignment, not as a standalone deployed decision-making system. Any deployment in sensitive domains should include additional evaluation for bias, privacy, robustness, and domain-specific failure modes. In particular, users should validate performance on the target population and application setting, avoid using the method for high-stakes decisions without human oversight and accountability, and ensure that data collection and use comply with consent, privacy, and legal requirements.

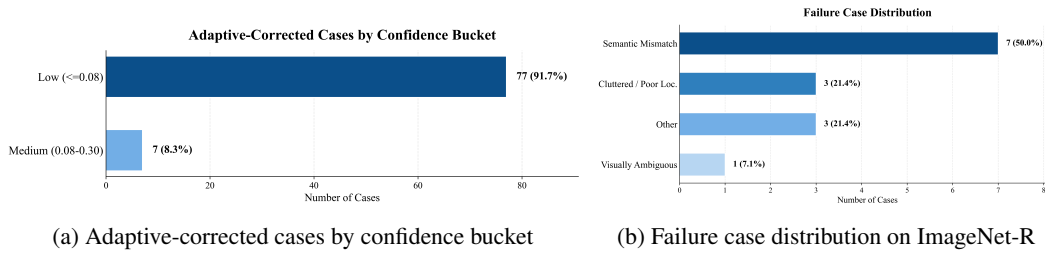


Figure 7: **Confidence-aware corrections and failure analysis under shift.** **Left:** Adaptive-corrected samples across confidence buckets. **Right:** ImageNet-R failure distribution under natural shift.

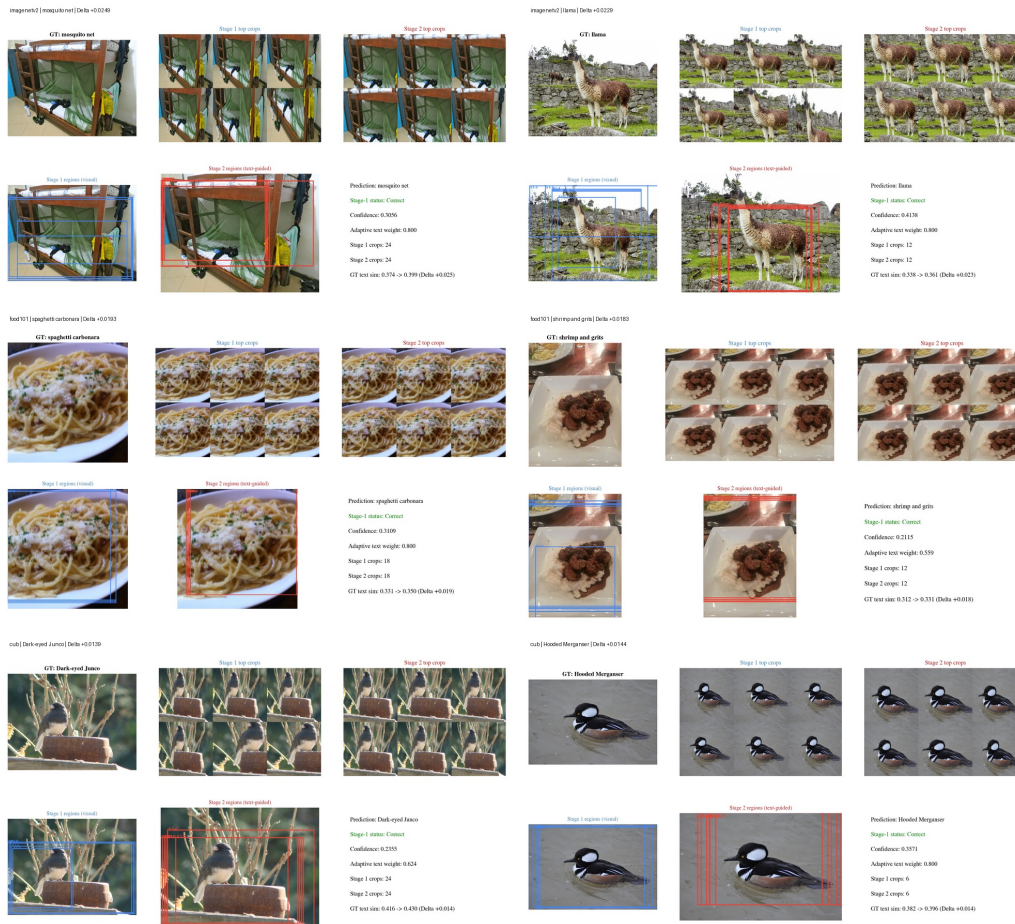


Figure 8: **Stage-wise visualization across ImageNet-V2, Food101, and CUB.** Representative examples from multiple datasets show a consistent pattern: Stage 1 identifies visually salient and object-centric regions, whereas Stage 2 shifts the selected crops toward regions that are more discriminative and semantically relevant for the predicted class. This qualitative trend suggests that the two-stage design consistently improves localized visual-text alignment across diverse recognition settings, including generic object recognition, food classification, and fine-grained bird recognition.

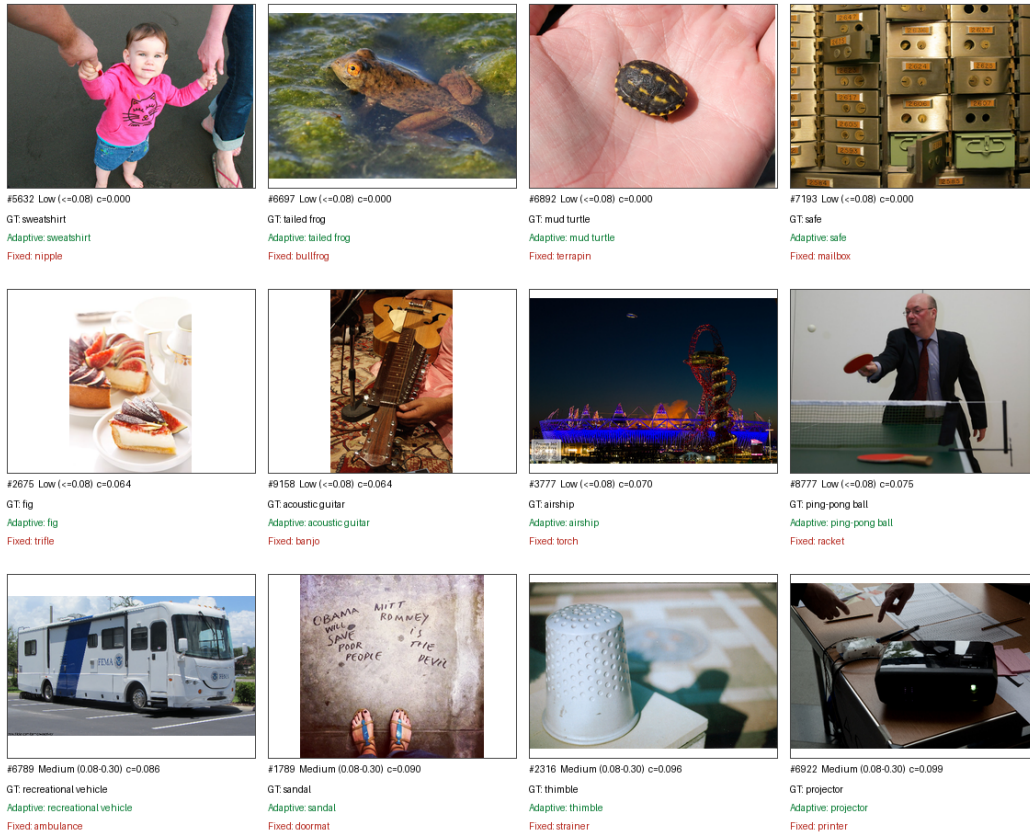


Figure 9: **Representative cases corrected by adaptive guidance.** Each example shows an image for which the adaptive strategy predicts the correct class while the fixed-guidance variant fails at inference time. The examples are grouped by intermediate-confidence bucket, illustrating that adaptive refinement is especially beneficial in many low-confidence cases, where aggressive fixed semantic guidance is more likely to overcommit to misleading visually plausible local evidence.



Figure 10: **Representative semantic mismatch failures on ImageNet-R.** The selected regions are locally plausible, but the text-side semantics emphasize misleading cues from the predicted text prototype under distribution shift conditions that do not support the ground-truth category.



Figure 11: **Representative cluttered or poorly localized failures on ImageNet-R.** The proposal set fails to isolate the truly discriminative region, leading the model to attend to incomplete or irrelevant evidence during inference under distribution shift, weakening later semantic refinement overall.

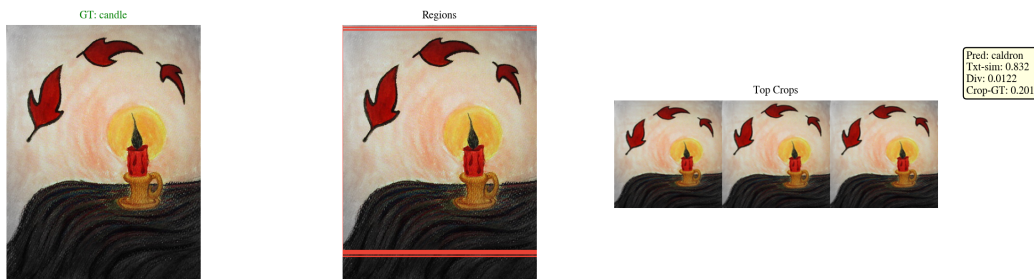


Figure 12: **Representative visually ambiguous failures on ImageNet-R.** Even after localized refinement, visually similar categories remain difficult to distinguish because they share highly overlapping local and semantically similar attributes under natural distribution shift at inference time.



Figure 13: **Representative failure cases categorized as other on ImageNet-R.** These examples do not fall cleanly into a single dominant error type, but still illustrate challenging cases for localized visual-text alignment under natural distribution shift with mixed semantic and localization errors.

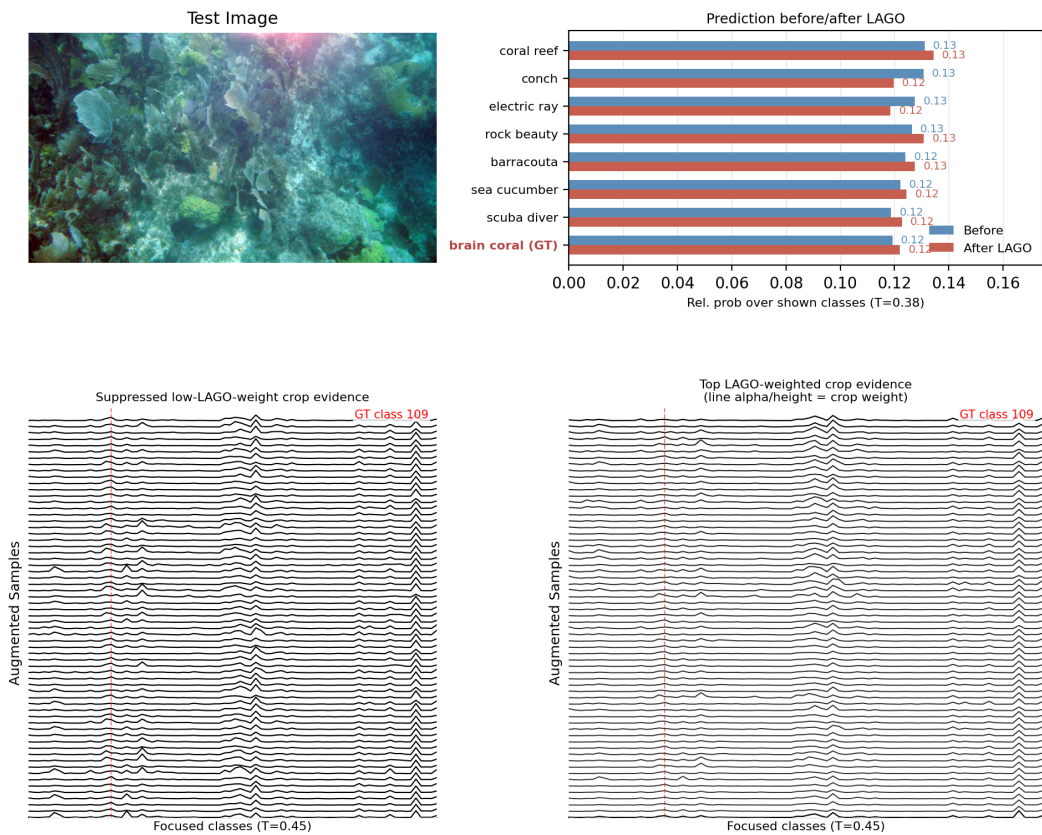


Figure 14: **Stage 2-only failure case on an underwater scene.** The ground-truth class is *brain coral*. Without class-agnostic visual initialization, Stage 2-only refinement produces diffuse evidence across related underwater categories. The ground-truth class is not separated after refinement, illustrating how unreliable early semantics can bias region selection and reinforce ambiguous predictions.

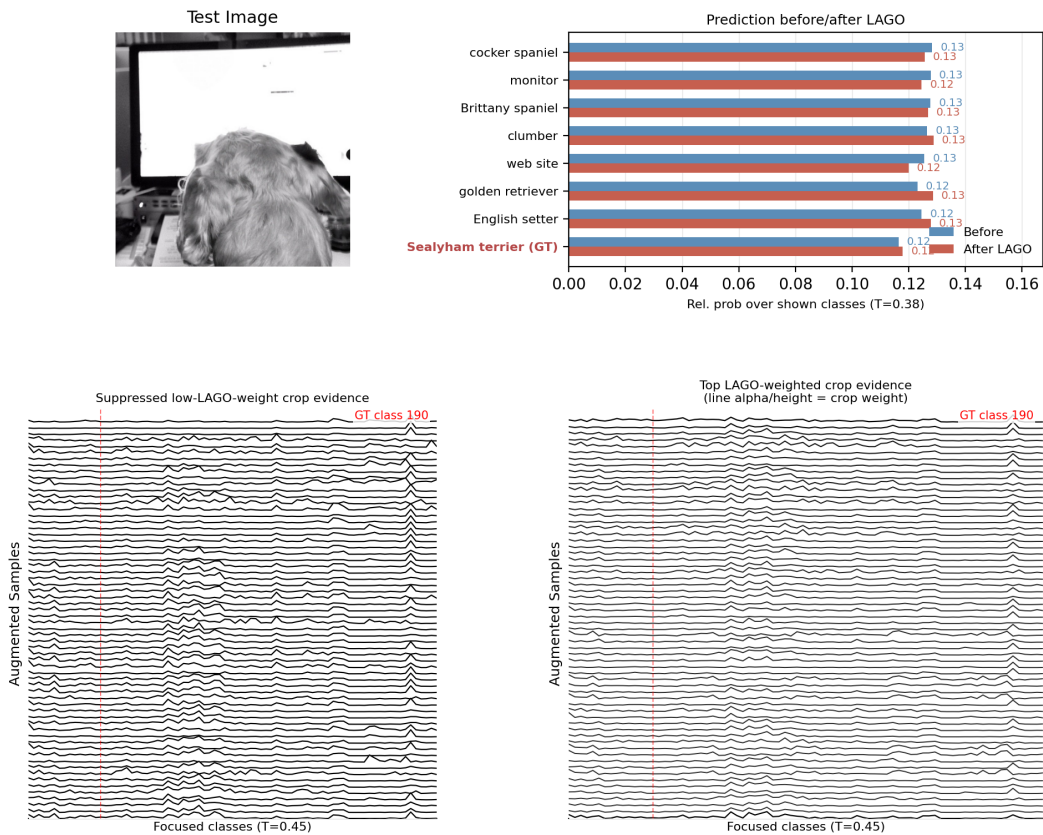


Figure 15: **Stage 2-only failure case on a fine-grained pet image.** The ground-truth class is *Sealyham terrier*. Without stable class-agnostic initialization, Stage 2-only refinement remains diffuse over related dog categories and confounding classes. This shows that applying semantic refinement from the start can overcommit to unreliable early evidence rather than isolate the discriminative region.

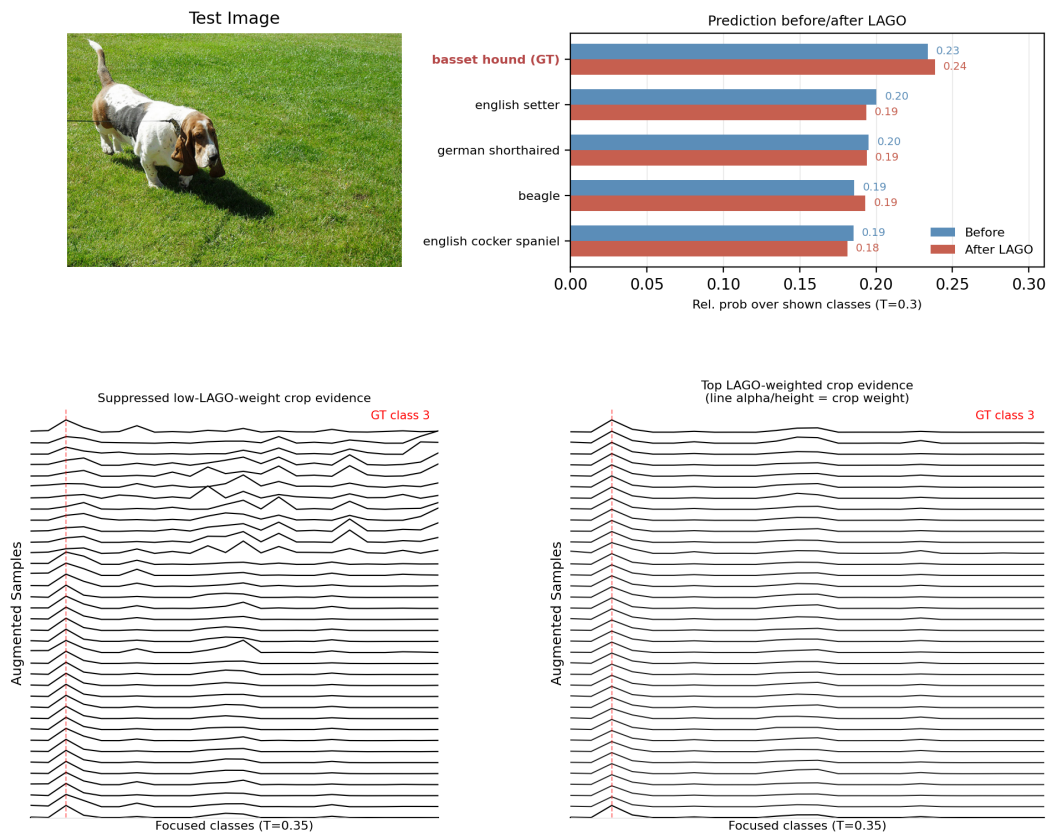


Figure 16: **Qualitative example of crop reweighting on Oxford Pets (basset hound).** LAGO **selectively** suppresses low-weight crops whose evidence is weak or less object-focused, while assigning larger weights to crops whose evidence is more concentrated around the ground-truth class. As a result, the prediction distribution after reweighting becomes more favorable to the correct class.

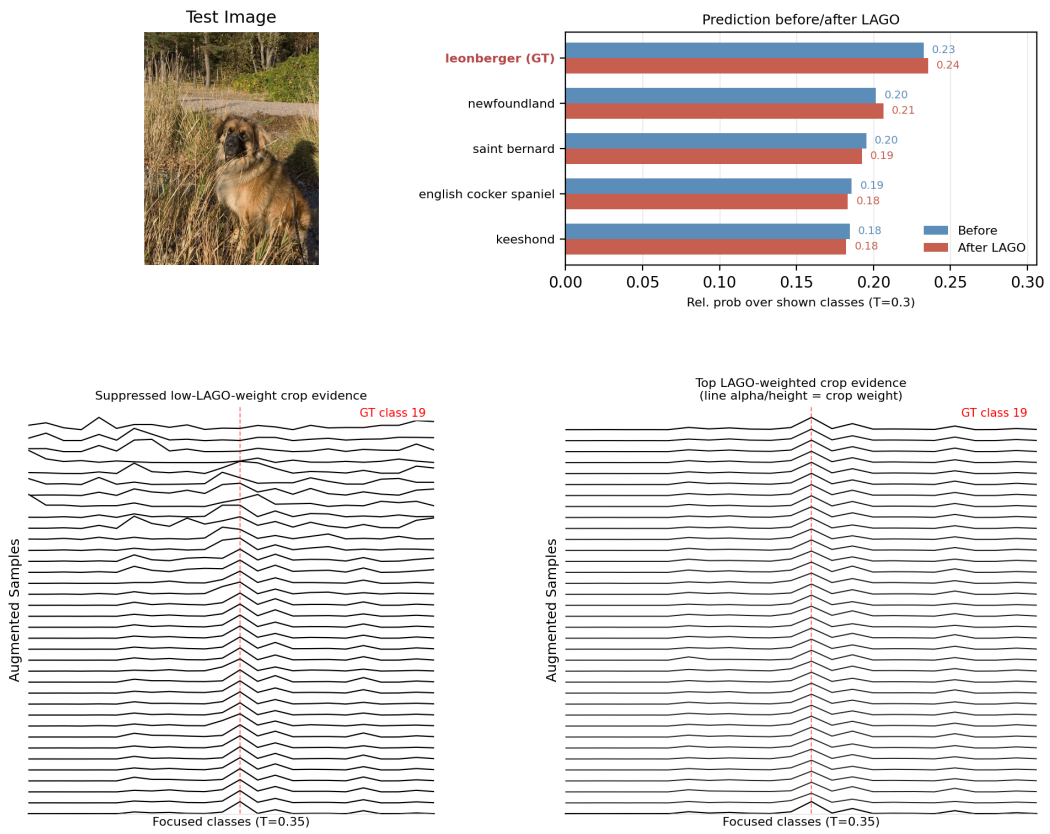


Figure 17: **Qualitative example of crop reweighting on Oxford Pets (leonberger).** Stage-wise reweighting suppresses weakly informative crop evidence and emphasizes regions whose predictions are more aligned with the target class, leading to a more concentrated final distribution.

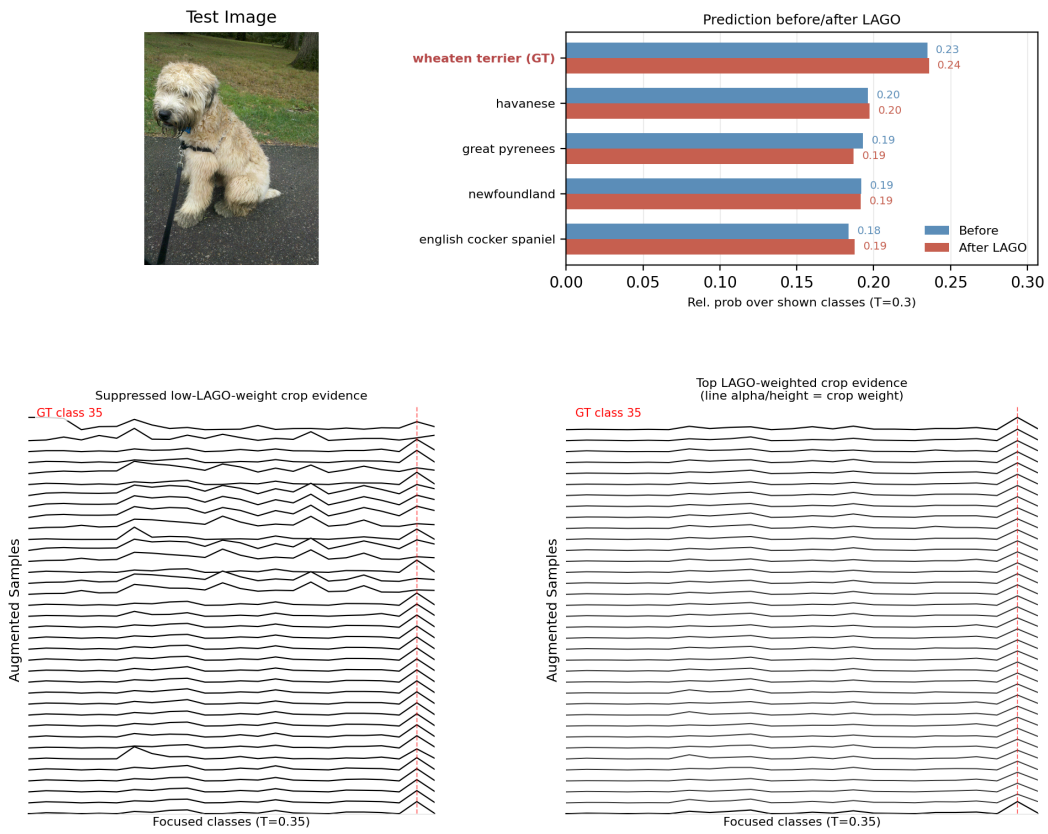


Figure 18: **Qualitative example of crop reweighting on Oxford Pets (wheaten terrier).** LAGO **selectively** downweights dispersed crop-level evidence and assigns larger weights to object-focused crops, improving the concentration of aggregated evidence around the ground-truth class.

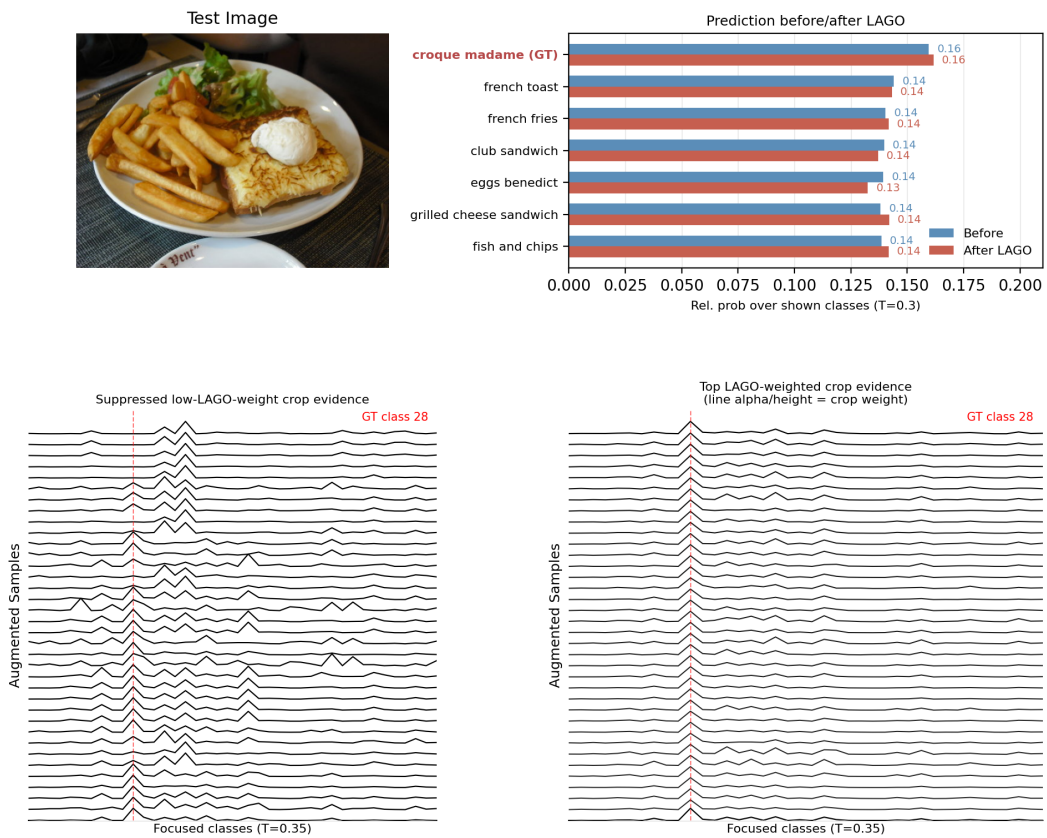


Figure 19: **Qualitative example of crop reweighting on Food101 (croque madame).** LAGO suppresses less relevant crop evidence and emphasizes crops that better capture the **visually and semantically** discriminative food structure, leading to a more reliable prediction after aggregation.

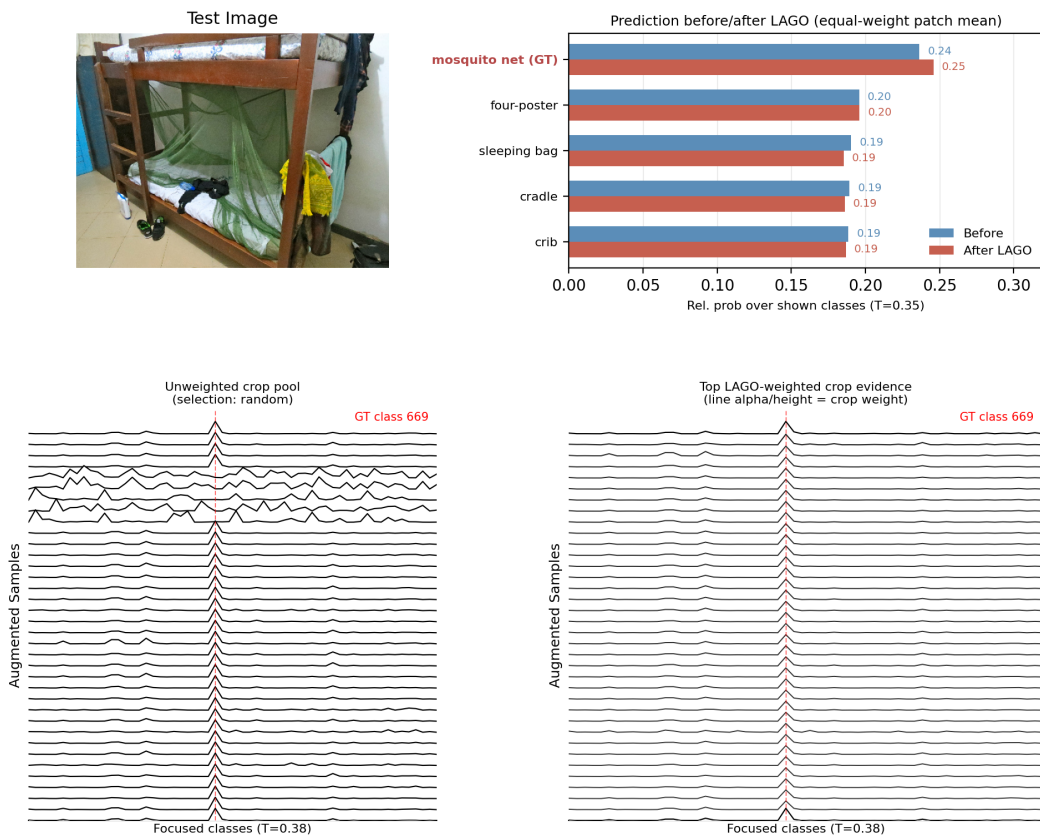


Figure 20: **Qualitative example of crop reweighting on ImageNet-V2 (mosquito net).** The weighted crop evidence after LAGO is more concentrated around the ground-truth class, illustrating how the method suppresses noisy crops and emphasizes semantically informative regions.

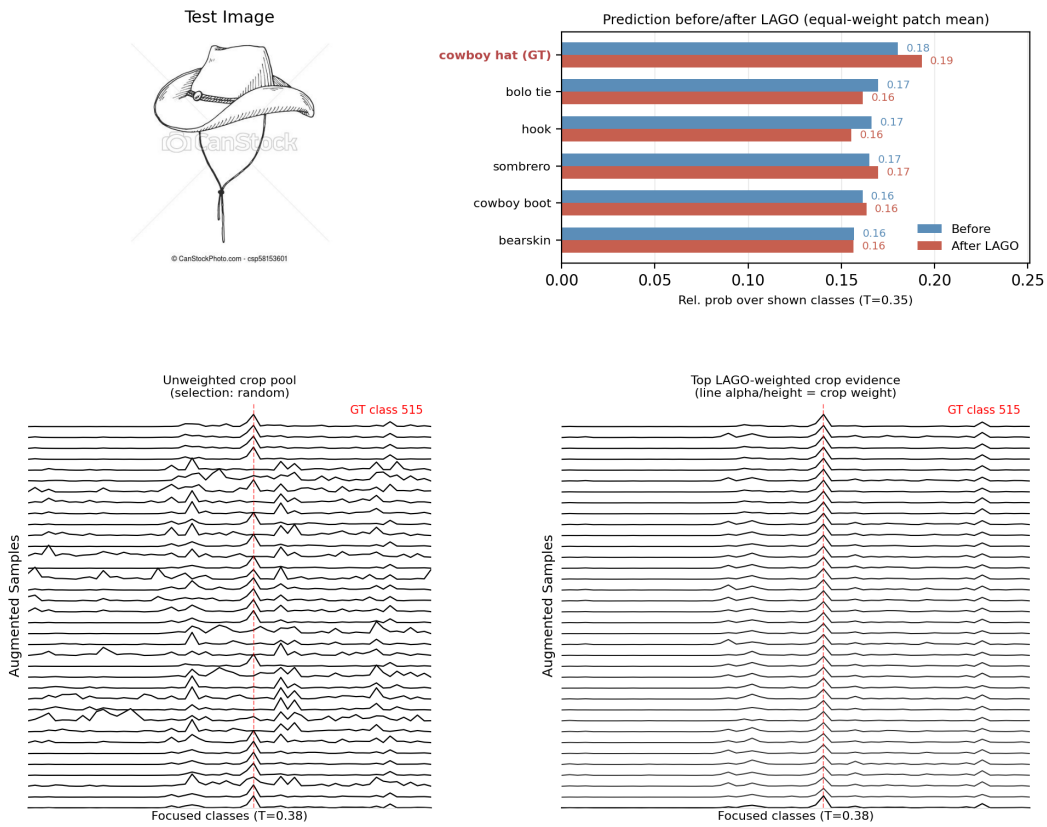


Figure 21: **Qualitative example of crop reweighting on ImageNet-R (cowboy hat).** In this stylized example, LAGO suppresses weakly informative crops and strengthens crop evidence that is more semantically consistent with the target object under natural distribution shift at inference time, leading to a clearer separation of the ground-truth class in the final prediction distribution overall.

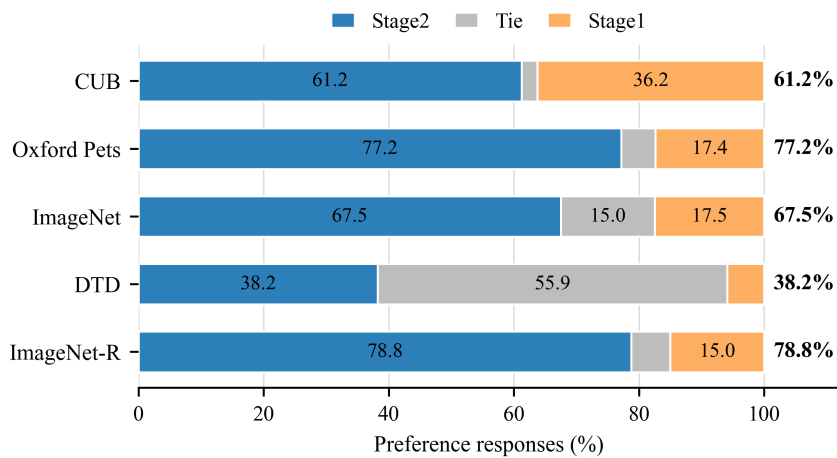


Figure 22: **Dataset-wise relative preference distribution over Stage 2, tie, and Stage 1.** Stage 2 is strongest on ImageNet-R and Oxford Pets, followed by ImageNet and CUB, while DTD shows many ties and remains favorable to Stage 2 among non-tie responses under the human evaluation protocol.

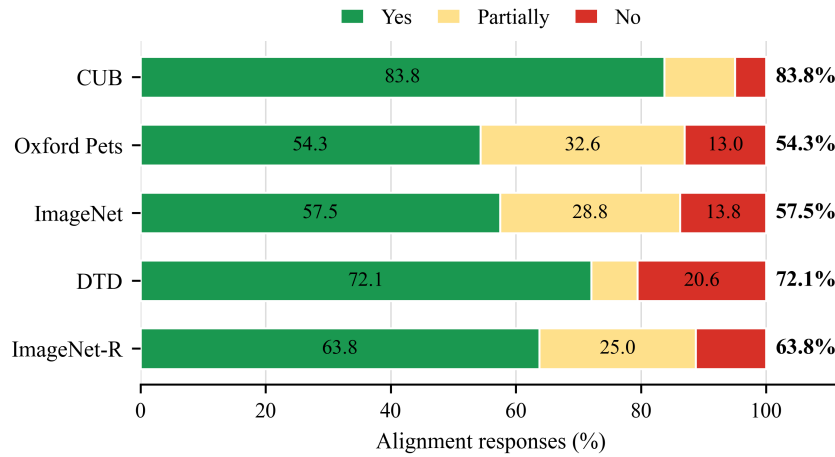


Figure 23: **Dataset-wise absolute Stage 2 alignment distribution over Yes, Partially, and No.** The strict alignment rate is highest on CUB, followed by DTD and ImageNet-R, while ImageNet and Oxford Pets are lower under the strict criterion in the human evaluation setting used here.

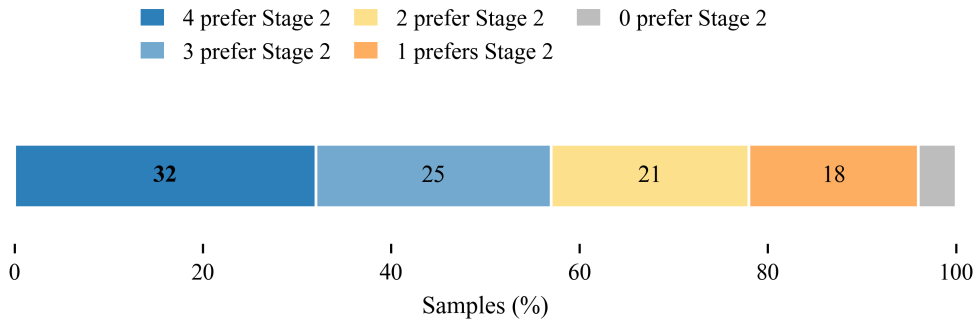


Figure 24: **Item-level support for Stage 2 preference across the four evaluators.** All four evaluators **consistently** prefer Stage 2 on 32/100 samples **overall**, a strict majority prefer Stage 2 on 57/100 samples **in this study**, at least half prefer Stage 2 on 78/100 samples **across all annotated items**, and at least one evaluator prefers Stage 2 on 96/100 samples under the human evaluation protocol.

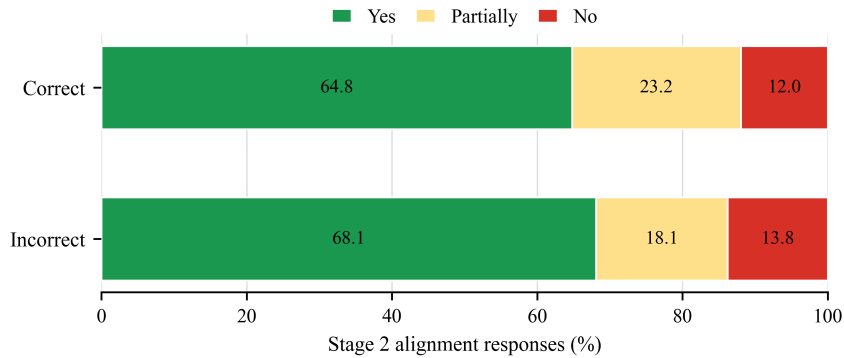


Figure 25: **Stage 2 alignment distribution conditioned on whether the final prediction is correct.** In this subset, human-perceived path plausibility does not simply track final decision correctness, especially in fine-grained or semantically ambiguous recognition settings at inference time.

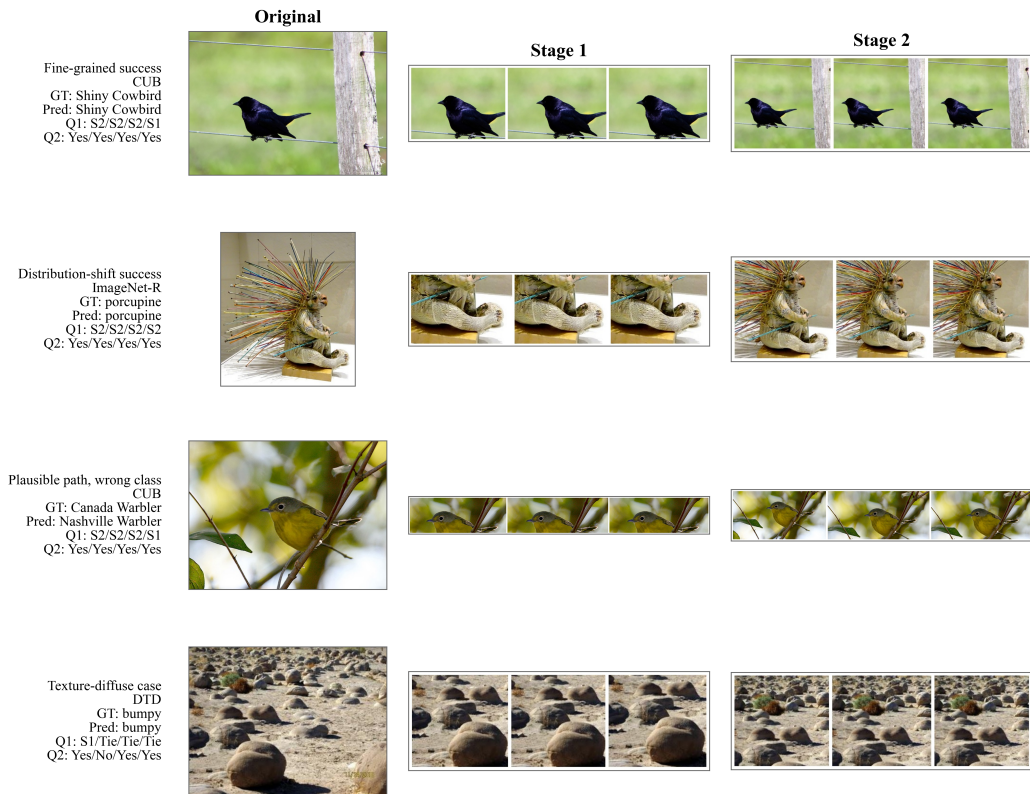


Figure 26: **Representative human evaluation examples.** Each row shows the image, Stage 1 regions, and Stage 2 regions, together with the ground-truth label, model prediction, and evaluator votes.